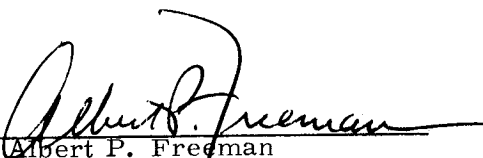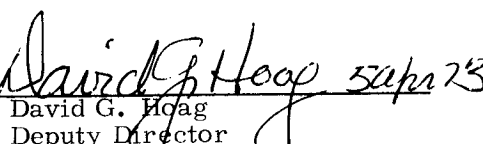# MASSACHUSETTS INSTITUTE OF TECHNOLOGY

AP LLO

GUIDANCE, NAVIGATION AND CONTROL

Approved: _____
Albert P. Freeman
Deputy Associate Director
Charles Stark Draper Laboratory

Approved: _____
David G. Hoag
Deputy Director
Charles Stark Draper Laboratory

R-757

OIL-FILM-PARAMETER INVESTIGATION

by

Edward P. Kingsbury

March 1973

MIT CHARLES STARK DRAPER LABORATORY

CAMBRIDGE, MASSACHUSETTS, 02139

ACKNOWLEDGMENT

The publication of this report does not constitute approval by the National Aeronautics and Space Administration of the findings or the conclusions contained therein. It is published only for the exchange and stimulation of ideas.

R-757

OIL-FILM-PARAMETER INVESTIGATION

ABSTRACT

The effects of speed, temperature, and starvation were investigated for conventional and retainerless Apollo gyro ball-bearing assemblies.

An apparatus for long-term monitoring of average retainer motions was developed.

Ball-pass forces were investigated and their connection with local changes in film thickness established.

by

Edward P. Kingsbury
March 1973

TABLE OF CONTENTS

LIST OF ILLUSTRATIONS

LIST OF ILLUSTRATIONS (Continued)

OIL-FILM-PARAMETER INVESTIGATION

1.   INTRODUCTION

       This report covers effort under the optical elastohydrodynamic (EHD) lubrication study program, Contract NAS 9-4065, during calendar year 1972. Specific effort during this reporting period concerned transparent-race experiments and retainer motion studies, continued from 1971, and ball-pass signal studies, started this year.

2.   TRANSPARENT-RACE EXPERIMENTS

       2.1   Test Setup and Calibration

              The counterrotating fixture (Fig. 1) was used to test the "good geometry" races received from MPB at the end of 1971.   This fixture is described in the previous report.[1]*   The glass races were cataloged according to the following system:

                      GR for Glass Race
                      Serial number
                      R or F for Relieved or Full dam
                      7 or 12 for the number of balls
                           in the assembly

Thus, GR16R12 describes glass race number 16 which had a ground dam (relieved) and a 12-ball group, i.e., no retainer.

       Although the inspection reports on these races were good, their Hertz zones generally showed large irregularities such as circumferential grooves. A typical Hertz "ellipse" is shown in Fig. 2 and may be interpreted as in the sketch in that figure.   Due to time limitations, these races were run as received (after coating with a semireflective layer of chromium) and all ran well.   Apparently, if geometry errors do not result in vibration (as the lobes on the sapphire races did), they do not have a bad influence on short-term performance.

----

*   Superscript numerals refer to similarly numbered references in the List of References.

HERTZ ZONE   TEST BALL

GLASS RACE
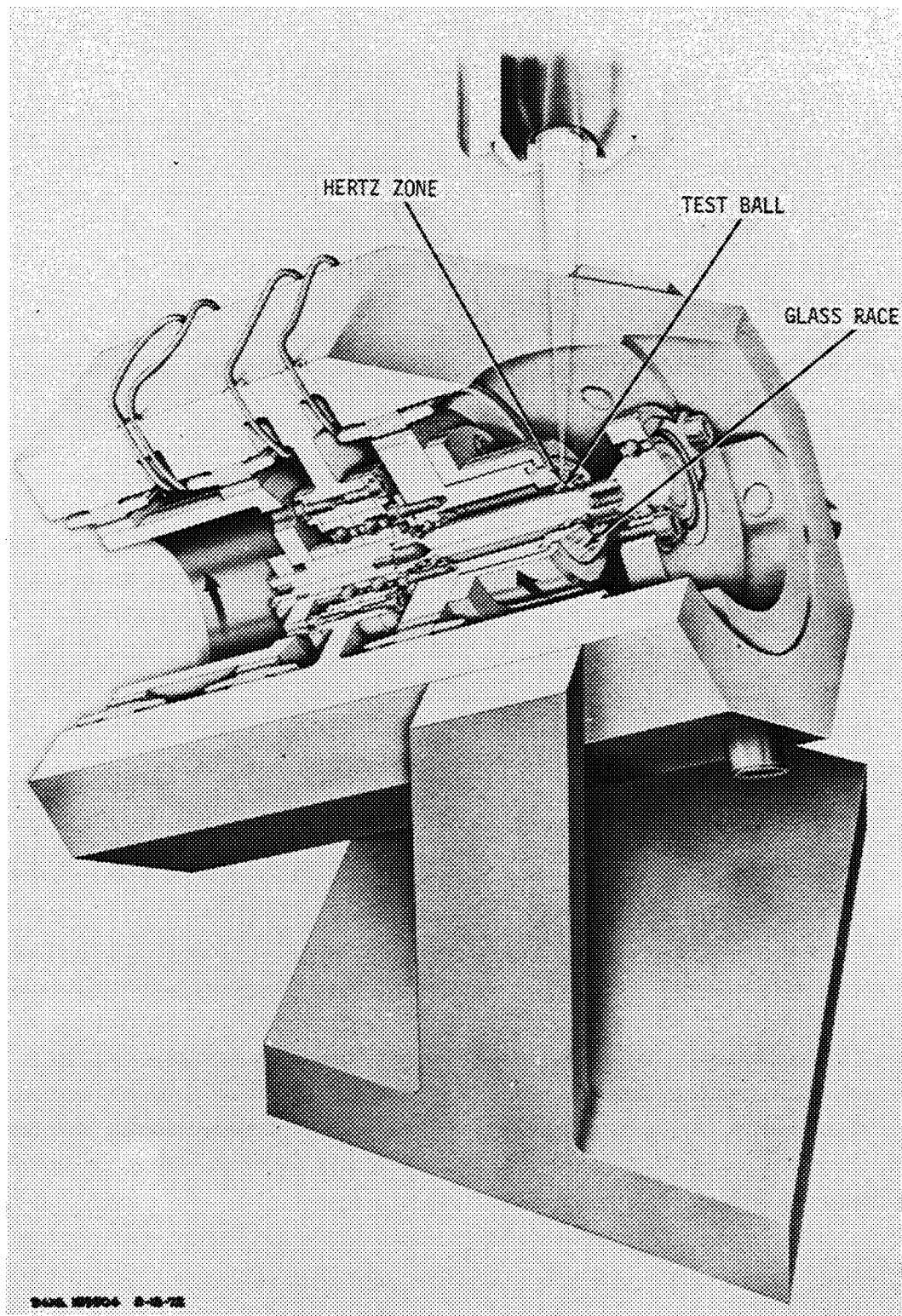
Fig. 1.   Counterrotation fixture.
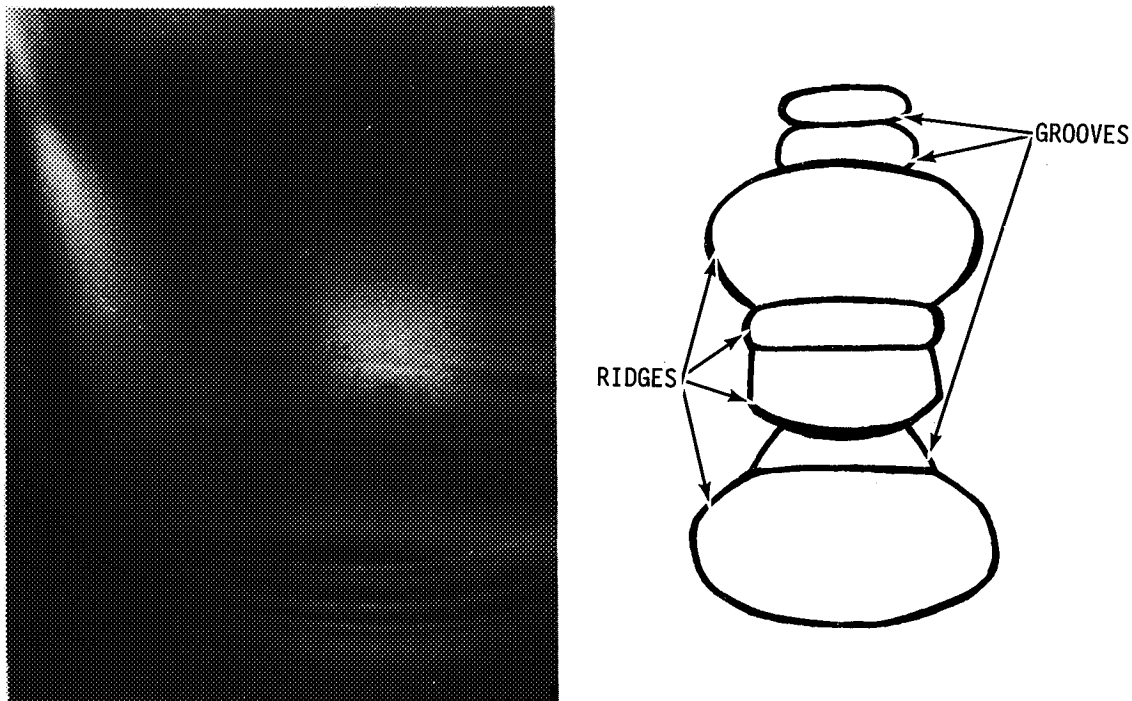
Fig. 2. Hertz zone.

The thickness of the EHD film was established by means of its color, which resulted from optical interference effects.[2] To calibrate the colors, a separate experiment was made using a 1-inch ball in contact in oil with an optical flat, and illuminated with the same source (Xeon stroboscope) as used in the EHD tests. Newton's rings in color were formed (Fig. 3) whose radii (r) (Fig. 4) could be measured. The corresponding film thickness (h) could be calculated according to the geometry of the contact.

$$\frac{h}{r} = 1 - \left[1 - \left(\frac{r}{R} \right)^2 \right]^{1/2} . \qquad (1)$$

The colors of the first two fringe systems and their corresponding thicknesses are as follows.

3
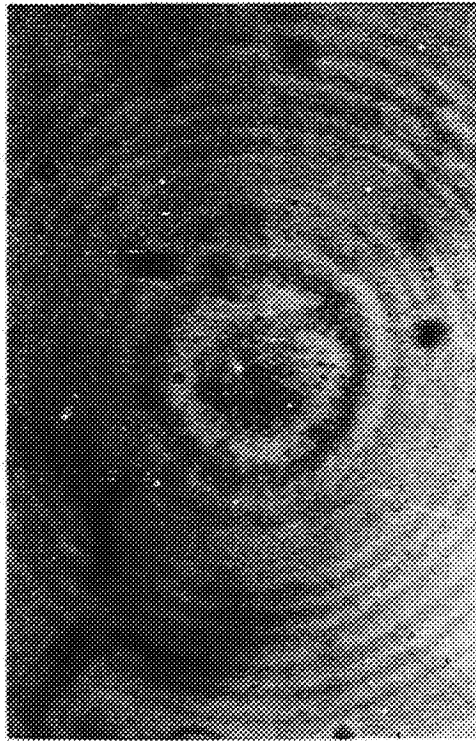
Fig. 3.   Newton's rings.

r

h

R = 0.5000 inch

×
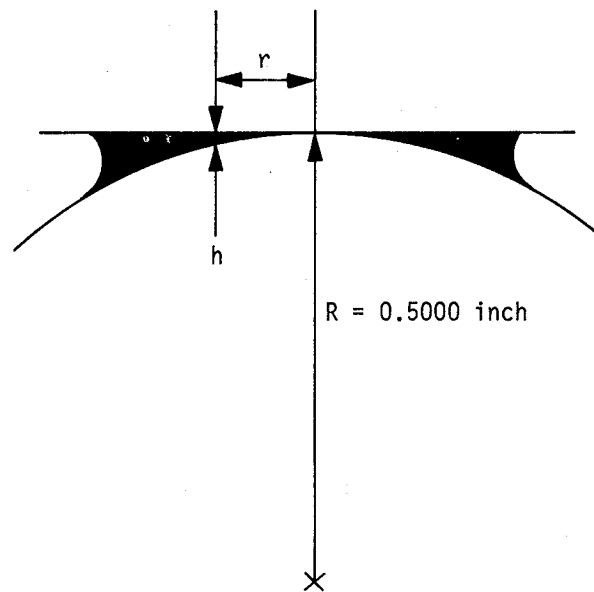
Fig. 4.   Geometry of Newton's rings.

Color	h (microinches)
slate	3
yellow$_1$	5
orange	6
dark blue$_1$	9
light blue	10
pale green	12
flat yellow	13
amber	14
blue$_2$	17

Beyond this depth, the colors in the calibration photos are too closely spaced to be useful.

A verbal description of the colors is unsatisfactory, but some of them are unmistakable, for example, the "flat yellow". By varying running conditions (e. g., temperature) and following color changes, the position of a particular color in the sequence can be established. Also, the change of color in a known groove (hence greater h) through the Hertz zone can be used. The resolution of the system is thus about 2 microinches up to depths of 20 microinches.

Two special fixtures were used to establish the normal load transmitted across the Hertz zone. Both took advantage of the visibility of the Hertz ellipse. The first system dead weight loaded the whole assembled bearing (Fig. 5); the second used a yoke and pendulum to load the outer against one ball and was much simpler to use (Fig. 6). Since both methods gave the same results, the pendulum method was adopted. Figure 7 shows the increase in the size of the Hertz ellipse for a single contact at equivalent preloads of 1 and 2 lbf. Using pictures like Fig. 7, the load spacer could be lapped and the Hertz ellipse adjusted to get any desired preload. In this report, all tests were done at an equivalent total preload of 1 lbf.

2.2 Film-Thickness Measurements

Results are discussed for the effect of speed, retainer temperature, and starvation on film thickness. To some extent, these parameters are inter-related. For example, a bearing cannot be run in air at higher speeds without also increasing its convective cooling rate, thus affecting its bulk temperature. For the Apollo test wheel, it was necessary to control the heat to the fixture to maintain a given retainer temperature. Similarly, both increased temperature and increased centrifugal field cause higher bleed rates within the retainer, affecting the rate of oil supply to the wear track and hence starvation. Attempts were made to separate out these various effects as discussed below.
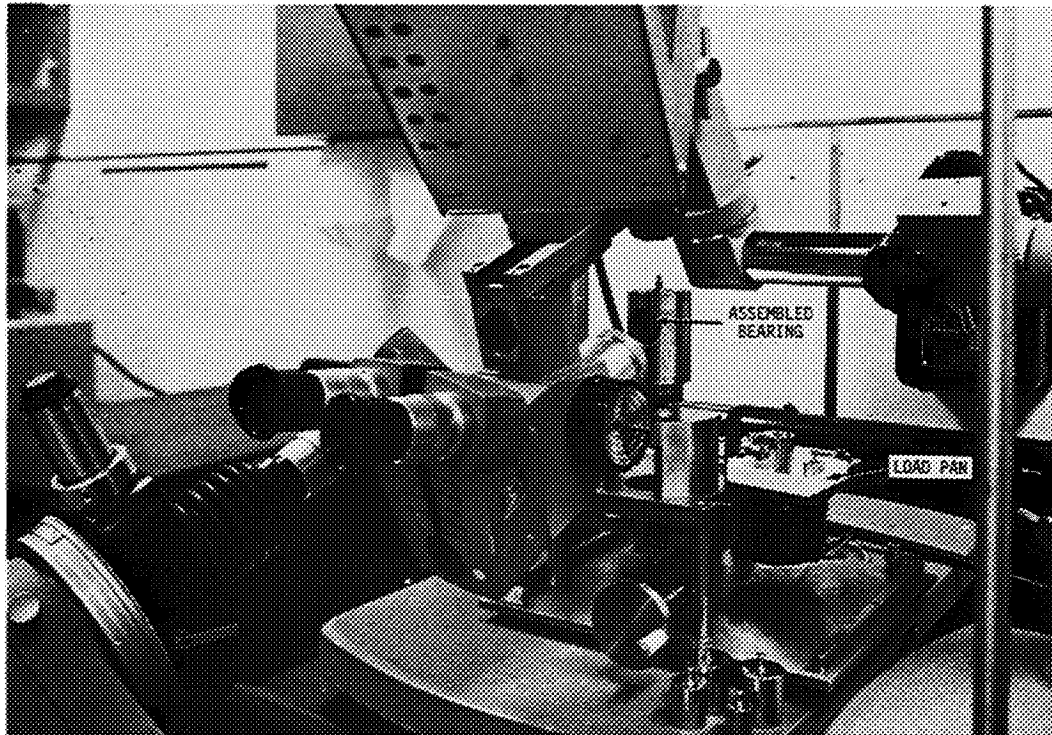
Fig. 5.   Complete bearing load calibration fixture.

Fig. 6.   Single-ball calibration fixture.
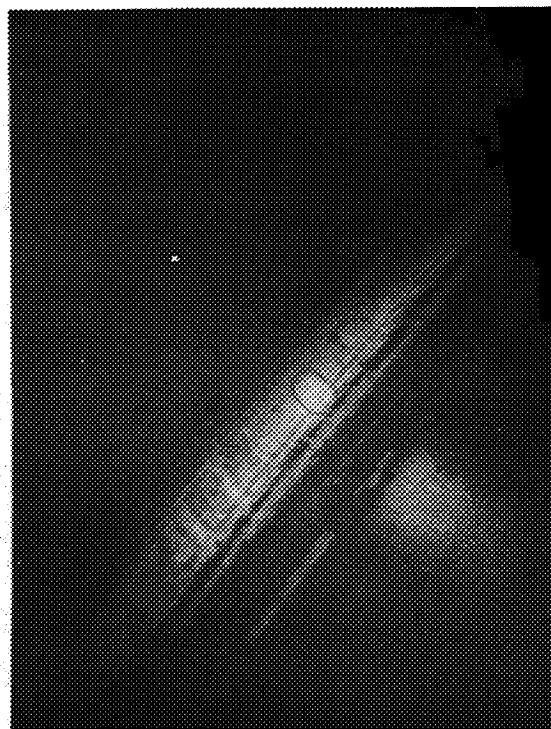
|1-1b preload|2-1b preload|

Fig. 7.   Hertz zone at two loads.

For the standard Apollo assembly procedures, which leave a minimum amount of oil in the bearing, it was found that neither speed nor retainer temperature has much effect on film thickness. Figure 8 shows the buildup of EHD film in GR11R7, very rapid at low speeds, constant, and then slightly falling at higher speeds. Similar behavior has been seen by Zeigler[3] and by Wedevan.[4] The dropoff has been attributed to an increase in contact temperature with speed, or alternatively, to an increase in starvation with speed.[4] Figure 9 shows the film thickness found in the same race at the full Apollo speed of 24,000 r/min. Figures 10, 11, and 12 show the increase in retainer temperature with running time after start-up and the accompanying film thickness for 2520, 4980, and 12,960 r/min. All these results show the relative insensitivity of starved film thickness to speed and retainer temperature.

Nonstarved EHD theory predicts that h should increase with increasing speed. The cross-flow analysis[1] for a starved contact predicts no dependence on speed. Basically, cross-flow says that in a starved contact, in-flow and leakage rates are equal and both are proportional to speed. Hence, speed cancels out.
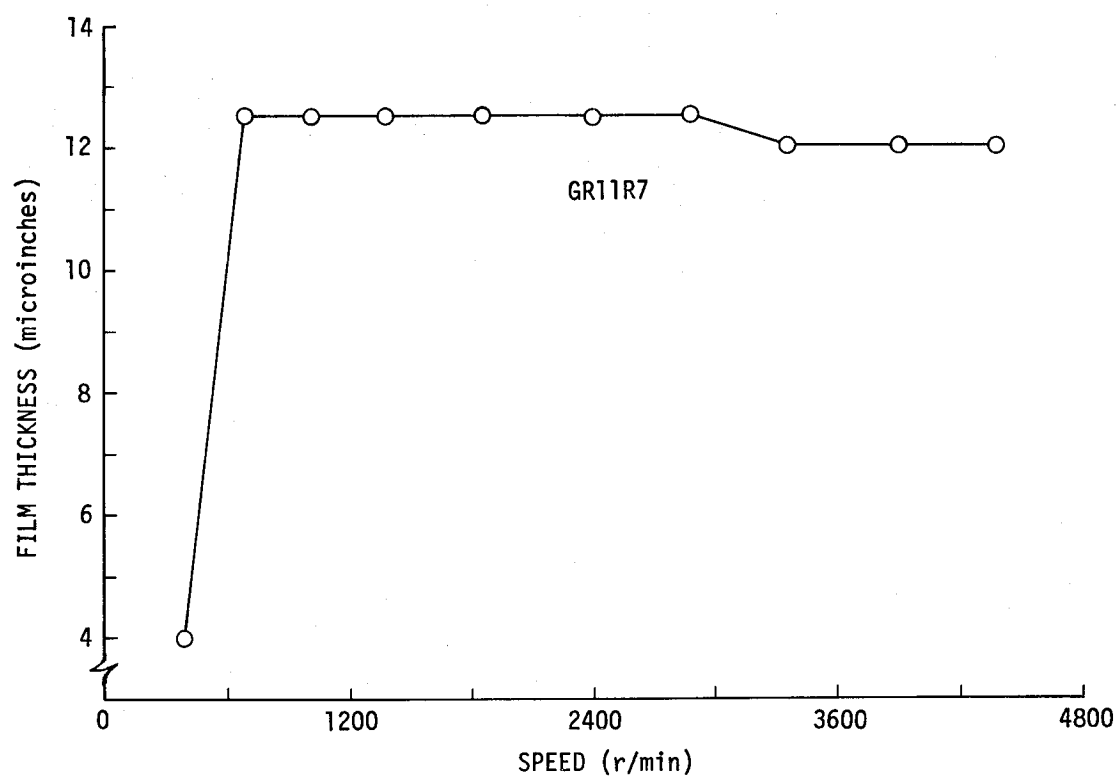
Fig. 8.   Film thickness versus speed.
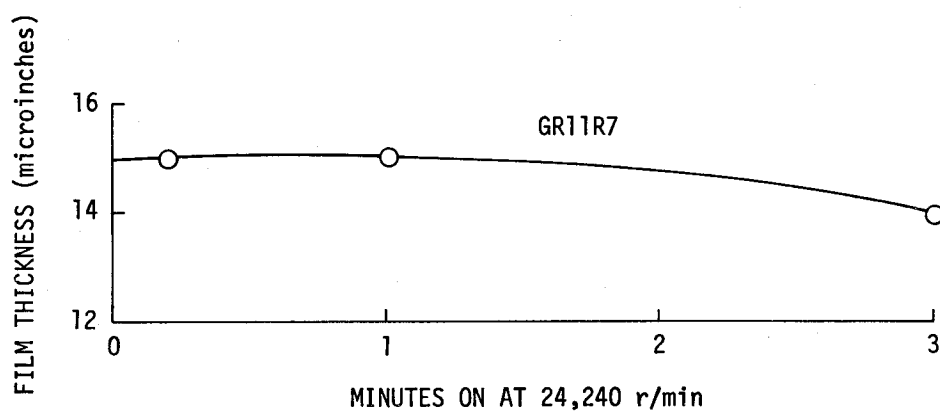
Fig. 9.   Film thickness versus time at 24, 240 r/min.

8
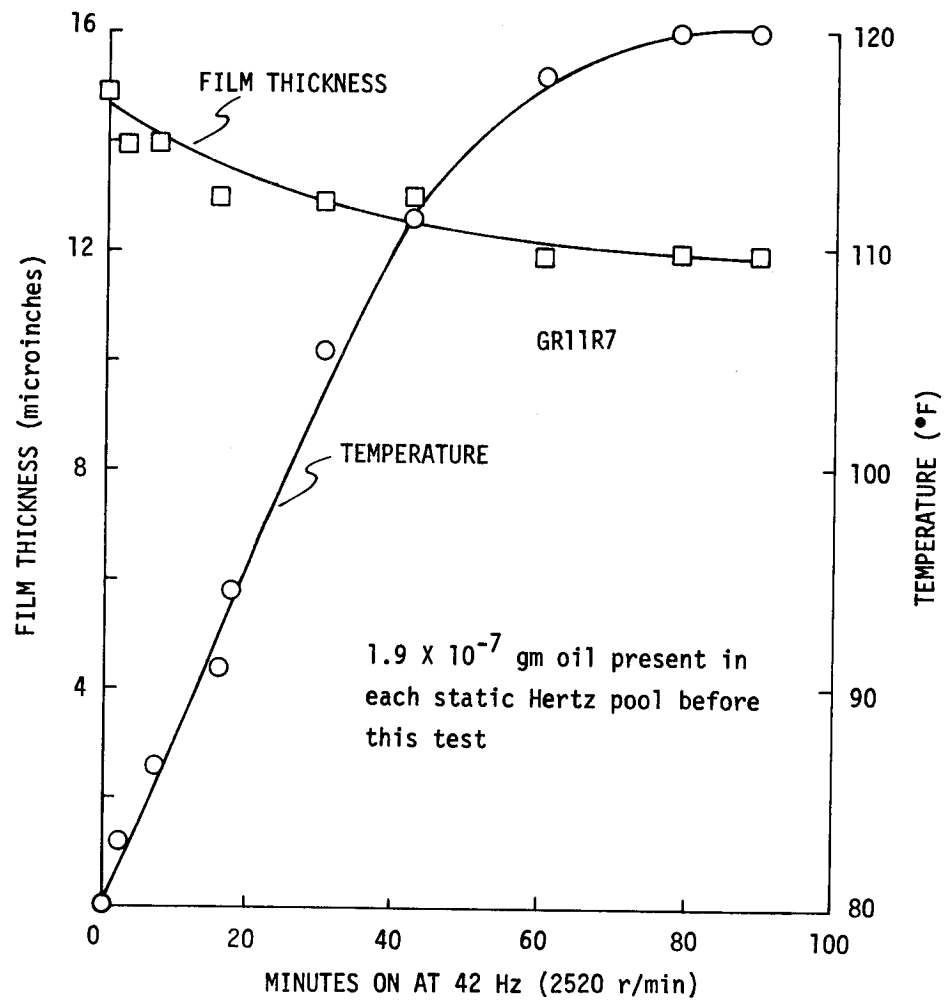
Fig. 10.   Film thickness and temperature versus time
at 2520 r/min.
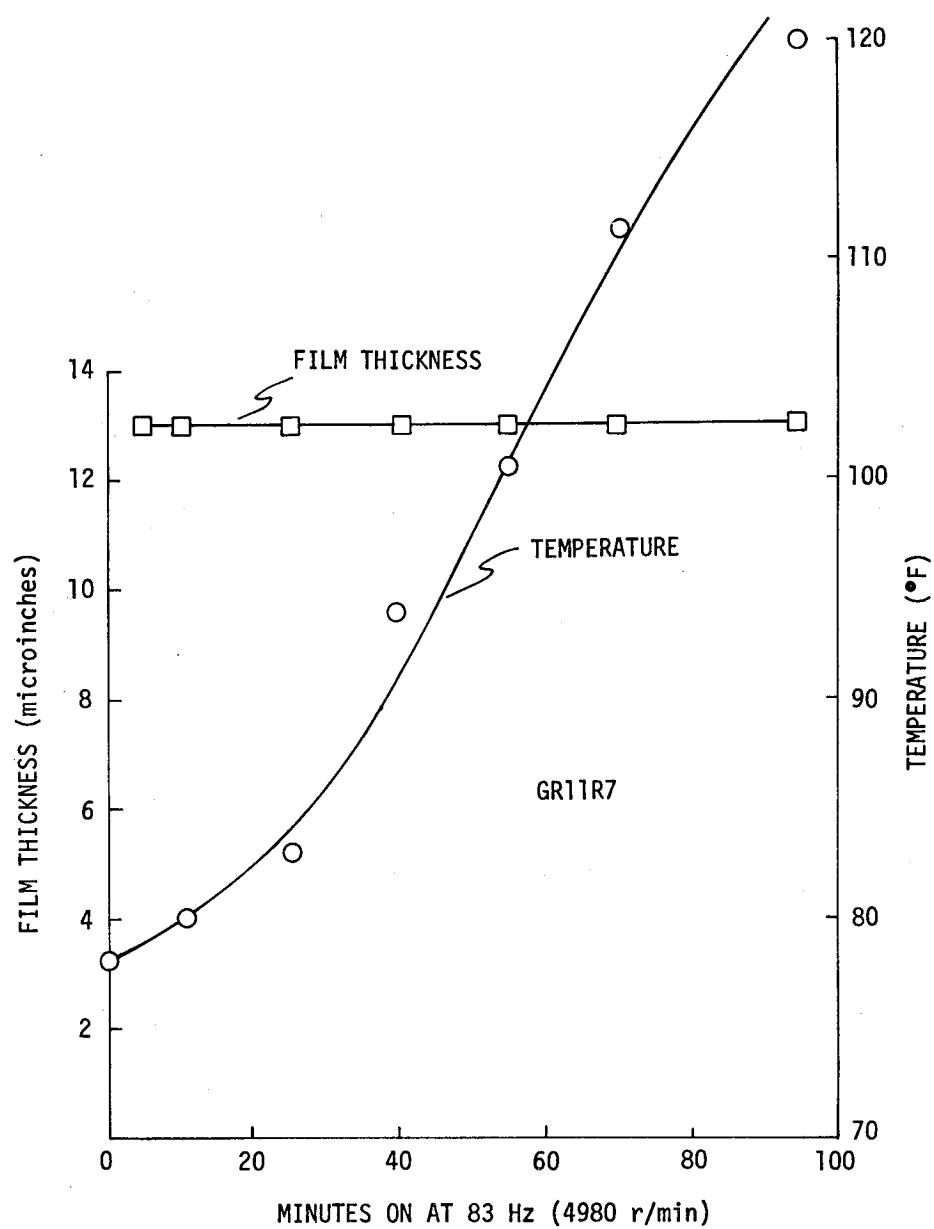
Fig. 11.   Film thickness and temperature versus time
at 4980 r/min.
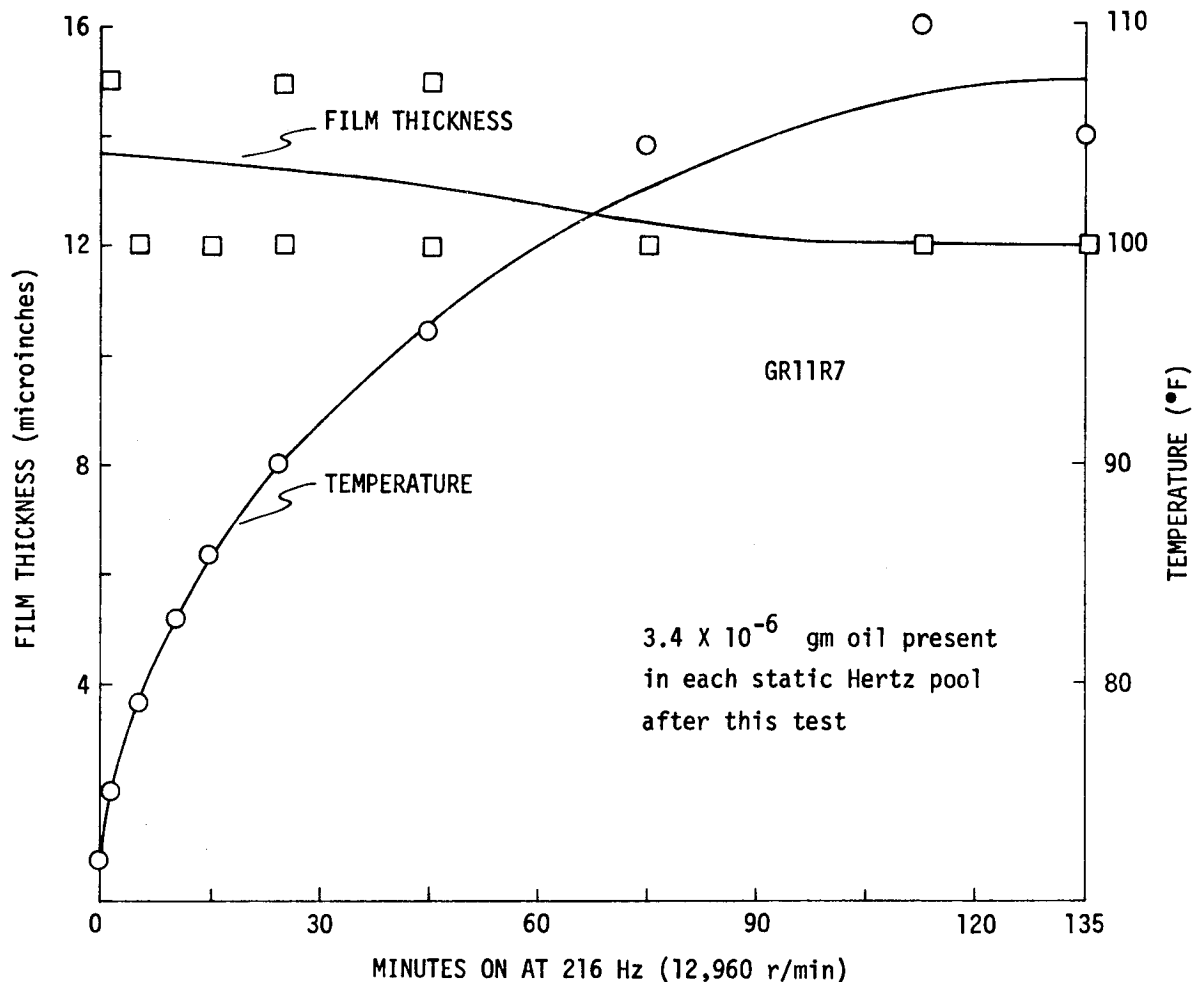
Fig. 12.   Film thickness and temperature versus time
at 12,960 r/min.

Temperature is brought into the classical EHD solution through its
influence on viscosity, which is assumed to be exponential, as is the pressure-
viscosity dependence. An increase in temperature then produces a large diminution
in viscosity, and a large reduction in film thickness is suggested. Cross-flow,
on the other hand, says nothing explicitly about the effects of temperature. But we
might expect the leakage rate from the Hertz zone (out-flow) to be proportional to
viscosity, and the flow through the retainer (certainly related to in-flow) as well,
again cancelling the effect of temperature. The trouble with such speculations about
temperature is that the relationship, if any, between the local temperature in the
contact and the bulk retainer temperature is unknown.

A basic discrepancy between cross-flow analysis and these experiments was detected as rapid step decreases in film thickness. Situations were often observed where a steady-state color in the Hertz contact showed flashes of another color, indicating rapid steps in film thickness away from and back to equilibrium. Steps in wheel hunt due to friction torque accompanied the color flashes. As presented in Reference 1, cross-flow says that abrupt decreases in thickness are impossible; evidently some extension of this theory is needed. For example, if the oil film on the balls is not uniform and if the spin axis of the balls should suddenly change,[5] new oil would be convected into or out of the wear track to produce these effects.

Following Horsch,[6] we take as a starvation criterion, "an increase in fluid supplied to a starved EHD contact results in an increase in film thickness." This may be compared with Cameron's,[2] "starvation exists when the inlet miniscus is less than 3 Hertz widths in front of the contact zone." The former is to be preferred as it is more direct. One could define the degree of starvation by a number such as

$$s = \frac{\partial h}{\partial q} \tag{2}$$

the rate of change of thickness with in-flow rate into the contact. At present, in-flows can only be established indirectly.[1, 3] For this investigation, it was intended to use the amount of oil stored in the pool around the Hertz zone at rest as a measure of the available lubricant. This "static pool mass" can be estimated from the width of the pool.[1] In a standard seven-ball assembly with retainer, however, it became apparent that the total oil stored in the bearing was shared between the retainer and the pools in a complicated way, depending upon the running history of the bearing. This is illustrated in Figs. 13 and 14, which plot the pool mass observed in GR11R7 as a function of time off after running. Oil slowly flowed into the pools from the retainer at a rate of 7.7×10^{-9} gm/h/contact as long as the temperature remained at 75°F. When the temperature was raised to 150°F, the oil flow increased to 4×10^{-7} gm/h/contact. When the temperature returned to 75°F, oil started to <u>leave</u> the pools, apparently being drawn back to the retainer. The involvement of the retainer is indicated in Fig. 14, which shows that the pool mass in GR1F12 (no retainer) remained constant with time off at 150°F.

Referring back to the h versus T runs on GR11R7, made successively at 2520, 4980, and 12,960 r/min (Figs. 10, 11, and 12), it is seen that the combination of increasing speed (centrifugal field) and high temperature in these runs resulted in more pool oil available at the end of the runs than at the beginning. This
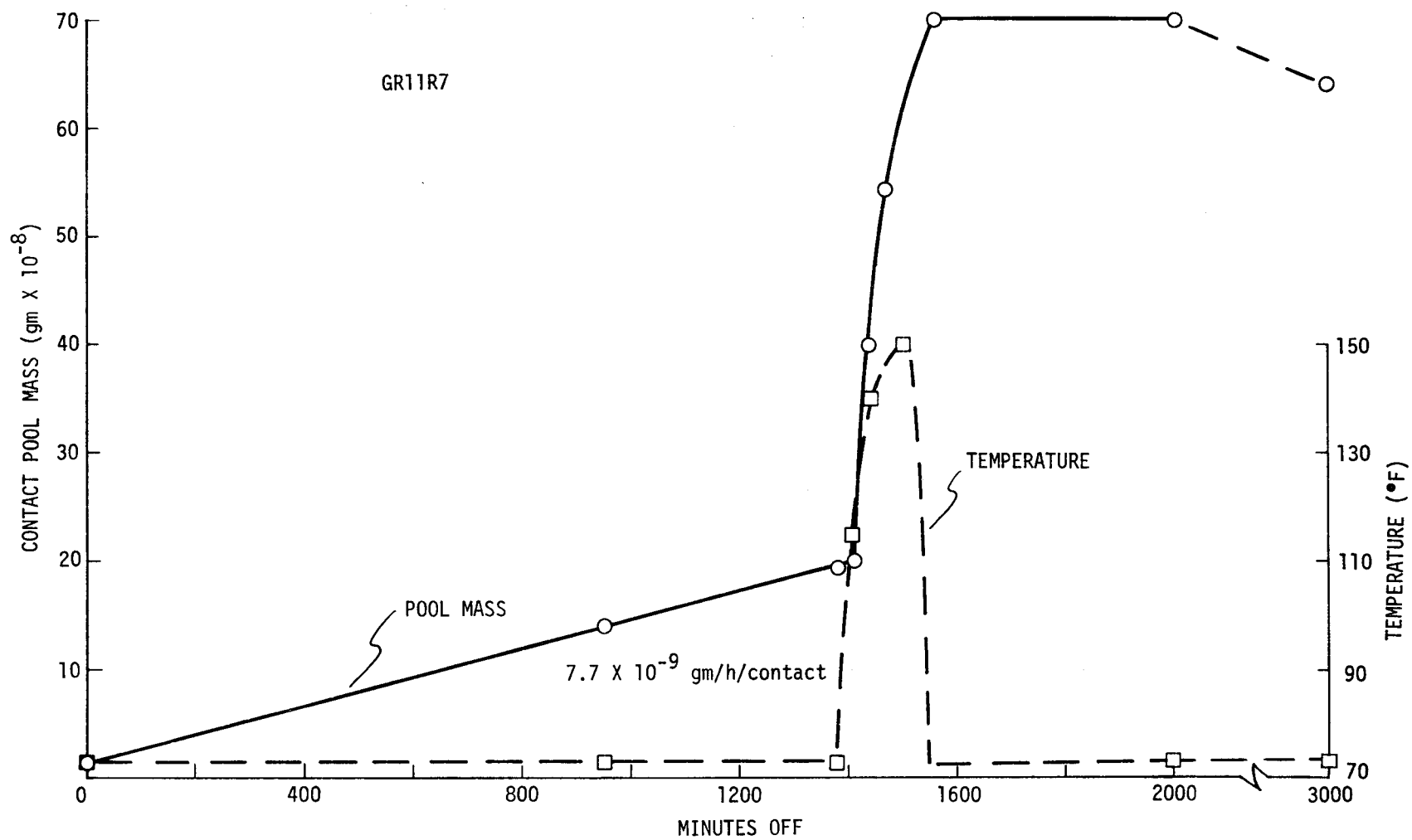
Fig. 13. Pool mass versus time off.

13
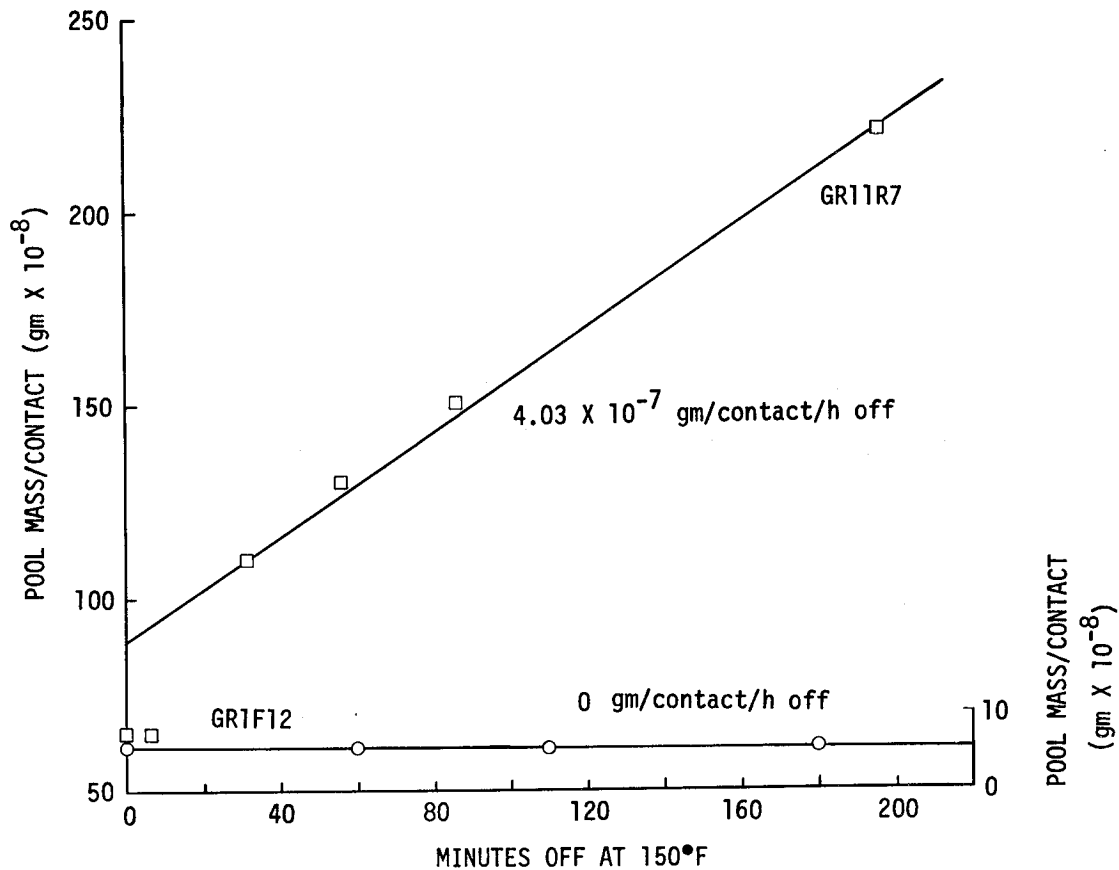
Fig. 14.   Pool mass versus time off at 150°F.

oil must have been bled from the retainer and presumably decreased the starvation of the contacts.   Compare this behavior with the data shown in Fig. 15, which plots static pool mass observed on GR16R12 (no retainer) after runs at 4920, 6960, and 14,760 r/min, all at 110°F.   h is constant at each speed, but decreases along with the static pool mass.   Apparently oil was being lost from the retainerless bearing as a result of running faster at the higher speeds, and this loss in available oil caused a decrease in film thickness according to the starvation criterion.   Using the data in Fig. 15, one can estimate that an oil loss of 28×10^{-6} gm caused a decrease in film thickness of 3×10^{-6} inches, and calculate a "starvation number" of

$$\frac{\Delta h}{\Delta m} = \frac{28}{3} = 9 \frac{\mu''}{\mu g} \tag{3}$$

14
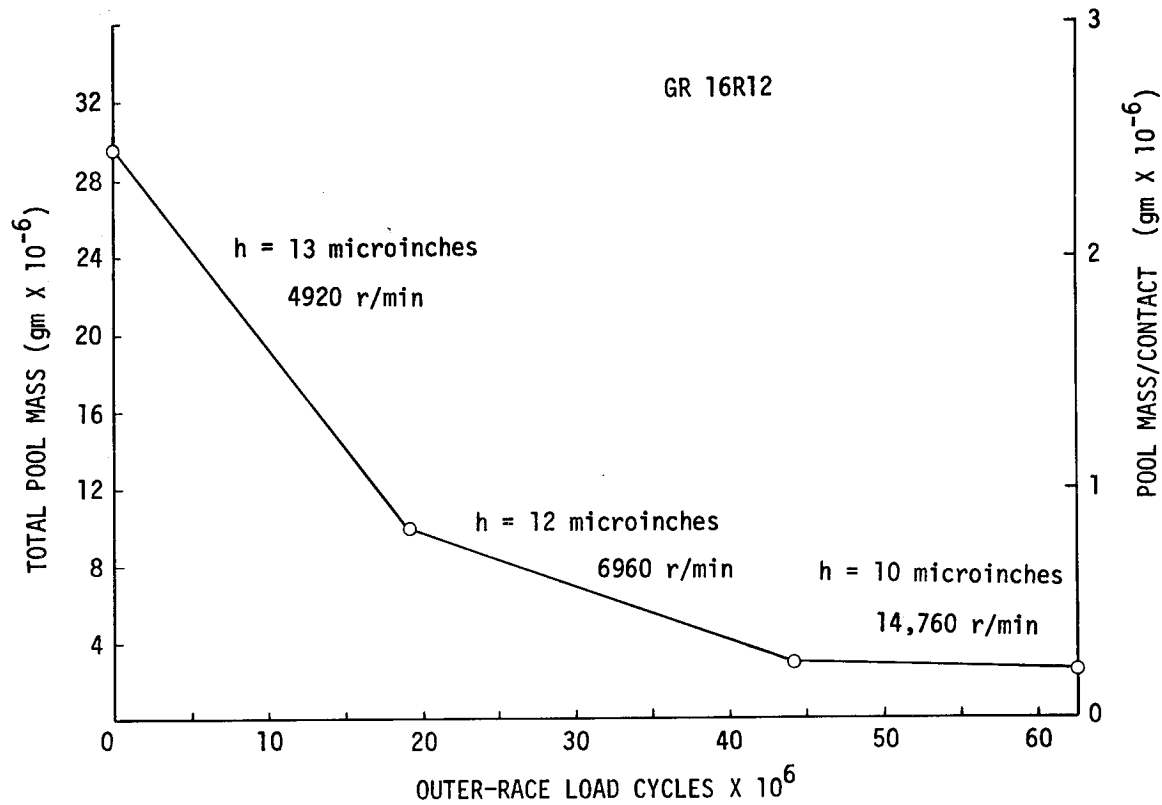
Fig. 15.   Pool mass versus outer-race load cycles.

From the geometry of the Apollo bearing, one can also estimate that the oil mass which is part of the wear track is

$$M = \frac{\pi}{2} \rho \, wh \, (Nd + 2E) \tag{4}$$

whence $dh/dm = 12 \, \mu''/\mu g$, in reasonable agreement.

Figure 16 is a plot of film thickness and temperature against running time at 4920 r/min for GR 16R 12. The amounts of pool oil before and after this run are also given. The measured decrease in thickness is evidently due to starvation rather than temperature since, when run the next day at room temperature, the thinner film was again measured. Here there is no complication due to retainer bleedout since there is no retainer in GR 16R 12.

Fig. 16.   Film thickness and temperature versus running time.

Some experiments with flooded contacts were made which showed the "horseshoe" closure in the contact outlet. Figure 17(a) shows the entering oil miniscus of GR14R7 at 5928 r/min and 120°F about 3 Hertz widths in front of the inlet. According to Cameron, this contact, which we call flooded, is starved. Even so, the film thickness is significantly greater than that resulting from the standard Apollo oiling procedures, being beyond the range of the color calibration. This is shown in Fig. 17(b), the same part of the GR14R7 at 4941 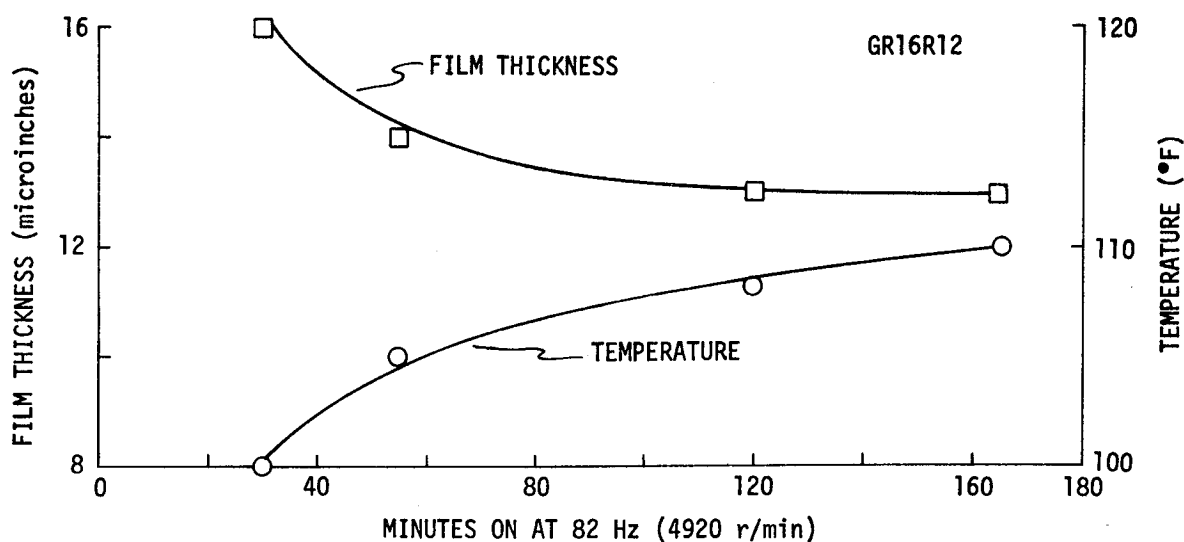r/min and 120°F but with the normal supply of oil. There is no inlet miniscus and very little internal detail. For the starved condition, variations in film thickness within the Hertz zone appear to be less than the calibration resolution of 2 microinches. For flooded conditions, with the exception of the horseshoe in Fig. 17(a), film detail is apparently caused by geometry defects in the glass race. The two circumferential grooves do not cause any diminution of the film by leakage. In fact, their main effect is to increase the average film thickness over the contact, as may be inferred in the original photographs from the colors within the grooves and the horseshoe.

2.3   Glass-Race Failures

Several glass races exhibited an aggravated spalling failure after (roughly) 100×10^6 loading cycles. Large volumes of glass were involved, as shown in Fig. 18, which is of a spalled area before and after solvent cleaning. Much of the detritus in Fig. 18(a) was polymerized oil which had formed just before the spall occurred. Signs of impending lubricant breakdown had been noted in

16

FLOODED   STARVED

(a)   (b)
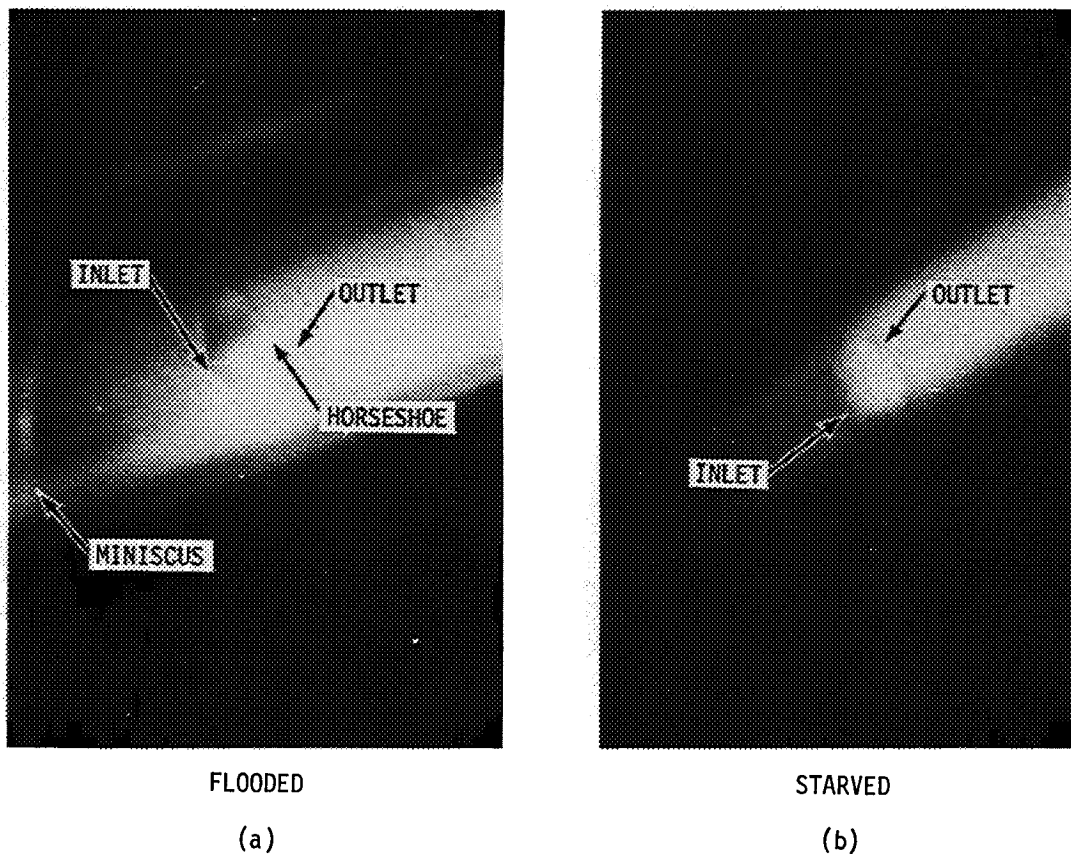
Fig. 17.   Hertz horseshoe.

earlier runs on this race, in the form of nonwetting at the edge of the stationary oil miniscus. This is shown in Fig. 18(c) in comparison with a normal Hertz pool, and indicates chemical changes in the oil or on the wear-track surface.

2.4   Summary

Starved EHD film formation is a complicated phenomenon where processes which take place far away from the contact govern its thickness. This is particularly true in a bearing that includes a ball retainer. Predictions of film thickness await better understanding of overall oil circulation within the bearing. The estimation of flow rate of new oil into the wear track is particularly important. The study of the role of ball spin in convecting new lubricant into the wear track should be pursued.

Thin EHD films do not prevent successful bearing operation even when local geometry variations are much larger than the film thickness. In particular, circumferential leakage through grooves does not seem to occur.

17

(a)
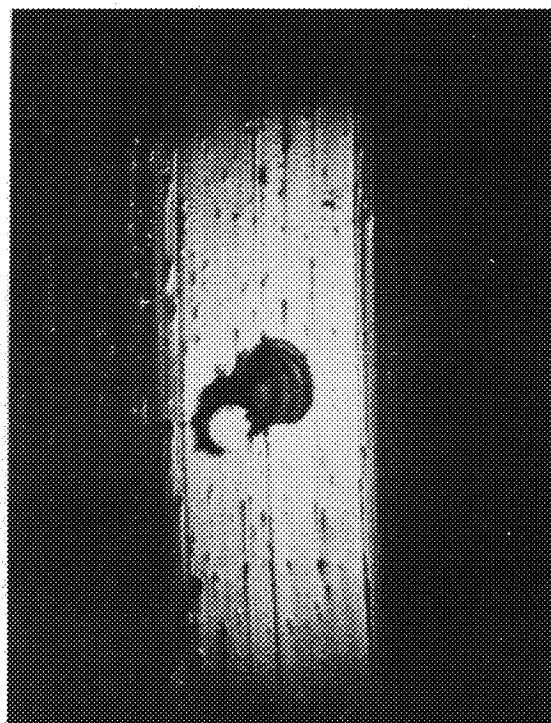
(b)

(c)

(d)

Fig. 18.   Spalls and lubricant breakdown.

18

3.   RETAINER MOTION STUDIES

3.1   Apparatus

The apparatus described in last year's report[1] for measuring instantaneous retainer motion was modified to record changes in average retainer motions over long periods of time. This information is a direct measure of disturbances in bearing perf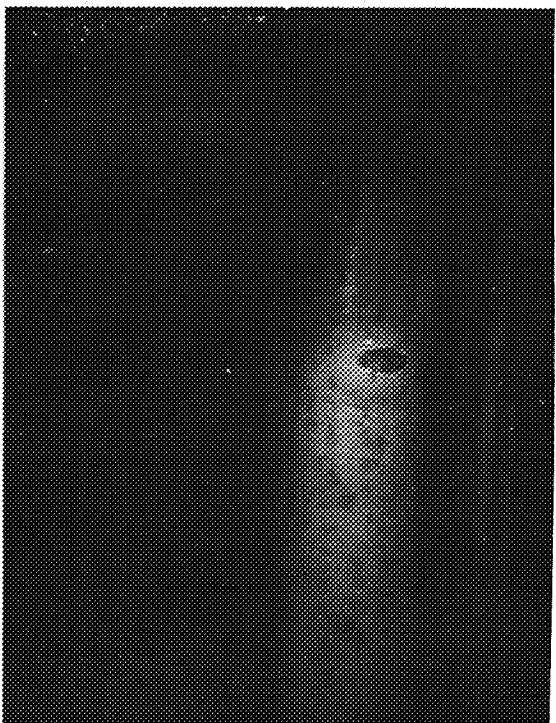ormance which are caused by the retainer and could be used in place of, or to supplement, the standard milliwattmeter trace as a diagnostic tool.

The apparatus measures light reflected from the face and edge of a moving retainer with separate fiber-optic probes located 180 degrees around the bearing from each other. The face (axial) probe is sensitive to axial or cocking motions, the edge (radial) probe to whirl. Both probes, when led into photo diodes, produce sinusoidal voltages whose major frequency component β is the retainer whirl rate (usually, but not always, equal to the ball-group-orbit rate[7]). The apparatus was modified to illuminate the retainer with fibre light ducts to reduce heating effects and to make illumination reproducible, and to monitor both positions on both retainers at once (Fig. 19).

In order to find changes in average retainer motion, the probe outputs are filtered to pass $\dot{\beta}$, demodulated and recorded. A retainer executing a stable eccentric rotation at $\dot{\beta}$ thus produces a straight line on the recording chart. Any change in the motion changes the $\dot{\beta}$ component in the edge (whirl) signal and shows up as a change in level on the recorded trace. Similar changes occur in the face signal if the retainer changes its axial position, starts a cocked motion, etc. Such records, being intimately connected with axial mass shifts, are a more direct measure of gyro performance than is the milliwattmeter trace.

3.2   Experimental Observations

Four examples of retainer motion traces will be given. In two cases, correlation with the milliwattmeter trace was found, in one case there was no correlation, and in the fourth a connection with total power demand (driving torque) was found. It was not possible to see if correlation with gyro performance existed.

Figure 20 shows simultaneous wattmeter and retainer motion traces during oil jags. In this experiment, the wheel speed was 24,000 r/min, resulting in a $\dot{\beta}$ of 243 Hz. The axial signal is fairly steady, meaning there is a large 243-Hz component present. This is interpreted, in the case of the Apollo bearing, as due to a stable cocking rotation (the high torque state in the "bimode" phenomenon). The radial signal shows large periodic drops in amplitude which are interpreted as "spasms" in the normal eccentric whirl rotation of the retainer. Both signals show

19
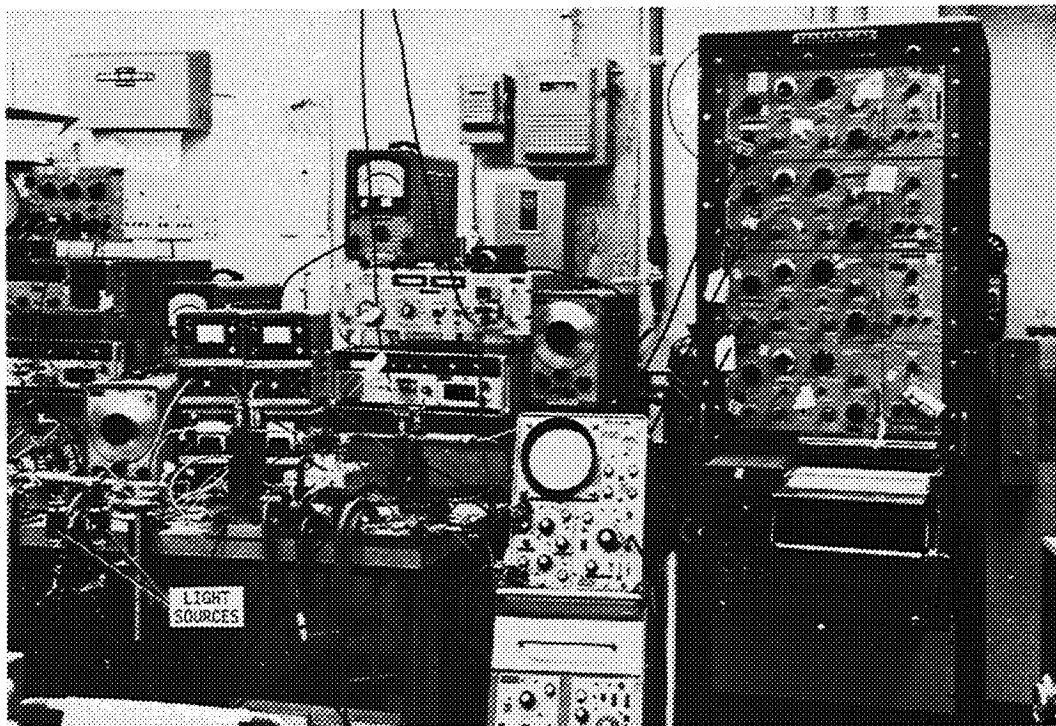
(a) Overall
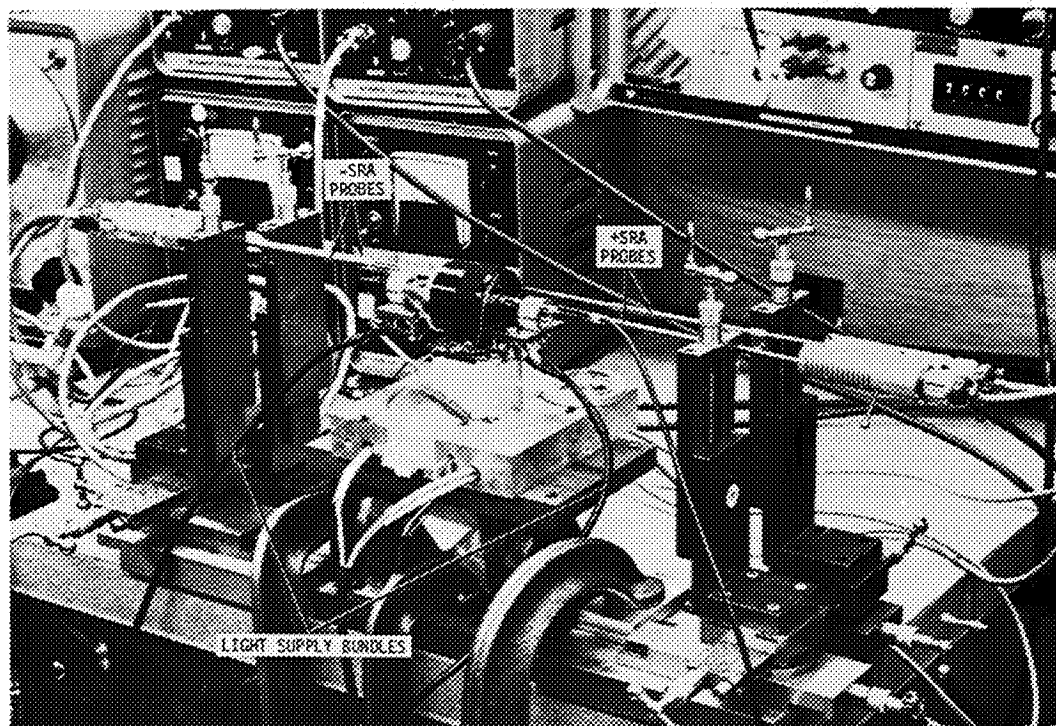
(b) Closeup

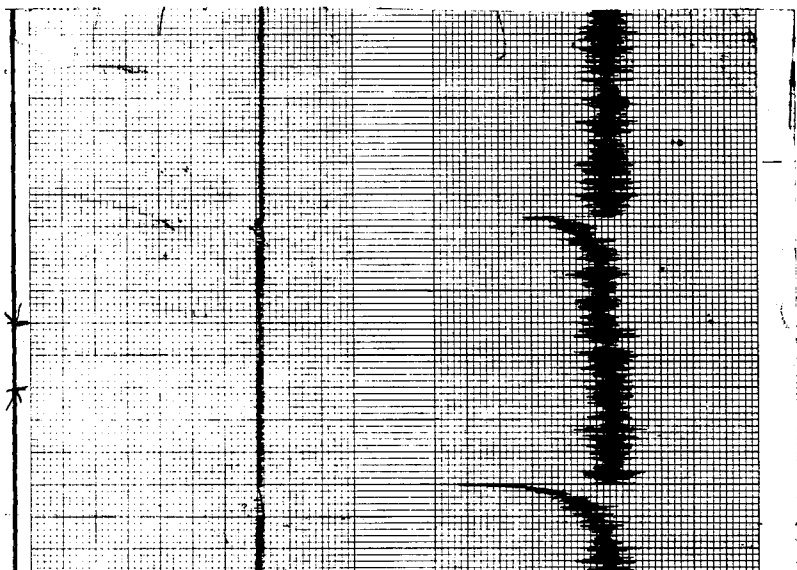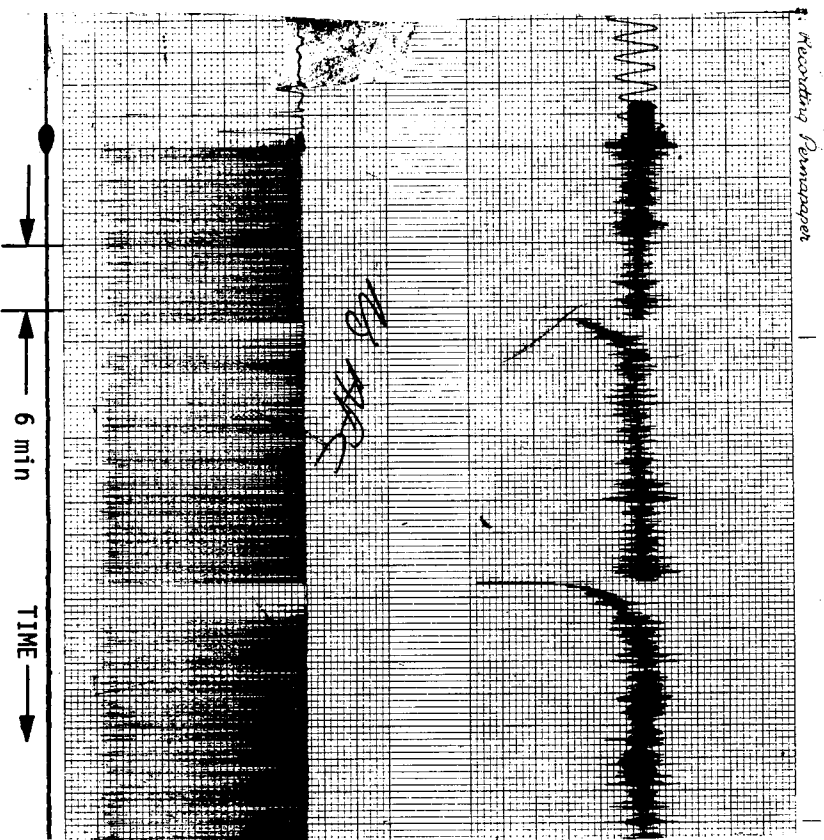Fig. 19.   Fibre optic probe fixture.

Fig. 20.   Retainer-average-motion trace during oil jag.

21

the influence of the oil jags, their effect being to quiet the disturbances. This is surprising since the standard model of an oil jag does not contemplate any effect on retainer motion. It could well be that the correlation which has been observed between drift rate and oil jags is due to an axial shift of the retainer center of gravity rather than to a shift of the whole wheel center of gravity on a thickened oil film, as the classical theory holds. More work is evidently required here.

Figure 21 shows the correlation between wattmeter and retainer motion during a bimode. The axial signals from both ends of the wheel are shown, the bimode occurring in the -SRA bearing. It is a typical bimode of 180 dyne-cm, the -SRA retainer going from a stable cocked rotation to an undefined "rattling" during the bimode. The motion of the +SRA retainer shows three motion regimes, is not influenced by the bimode, and in turn has no influence on the milliwattmeter trace.

Figure 22 shows some very short-term disturbances in the axial motion of one end of an Apollo assembly, which are not reflected in the milliwatt-meter trace. A picture of the unfiltered raw signals as seen on a dual-beam oscilloscope, taken at the same time, shows the one-to-one correspondence between the retainer-motion-trace record and the actual disturbances.

Figure 23 shows the differences in average retainer motion which occur in each end of an Apollo assembly when the wheel rotation is reversed. Also noted is the total electrical power required to drive the wheel in both directions, with a difference of 5%. Since there are four combinations of wheel and individual bearing rotations, it would appear that getting the most stable retainer rotations and least power wheel direction is a matter of some luck in standard assemblies.

3.3 Summary

It is believed that a refinement of these techniques could be profitably used in bearing screening for production gyroscopes. The light source and pickups could be permanently mounted in qualification fixtures and the retainer-motion traces obtained along with milliwattmeter data. Further information as to which types of retainer-motion disturbance would lead to changes in drift rate in the final gyro would be necessary and could be obtained without excessive difficulty on existing apparatus.

4. BALL-PASS SIGNALS

4.1 General Characteristics

Examination of the outputs from gyroscopes or bearing test devices shows that every pair of bearings produces a series of sinusoidal radial-force signals at frequencies given by

AVERAGE RETAINER AXIAL MOTION

-SRA
BEARING

+SRA
BEARING
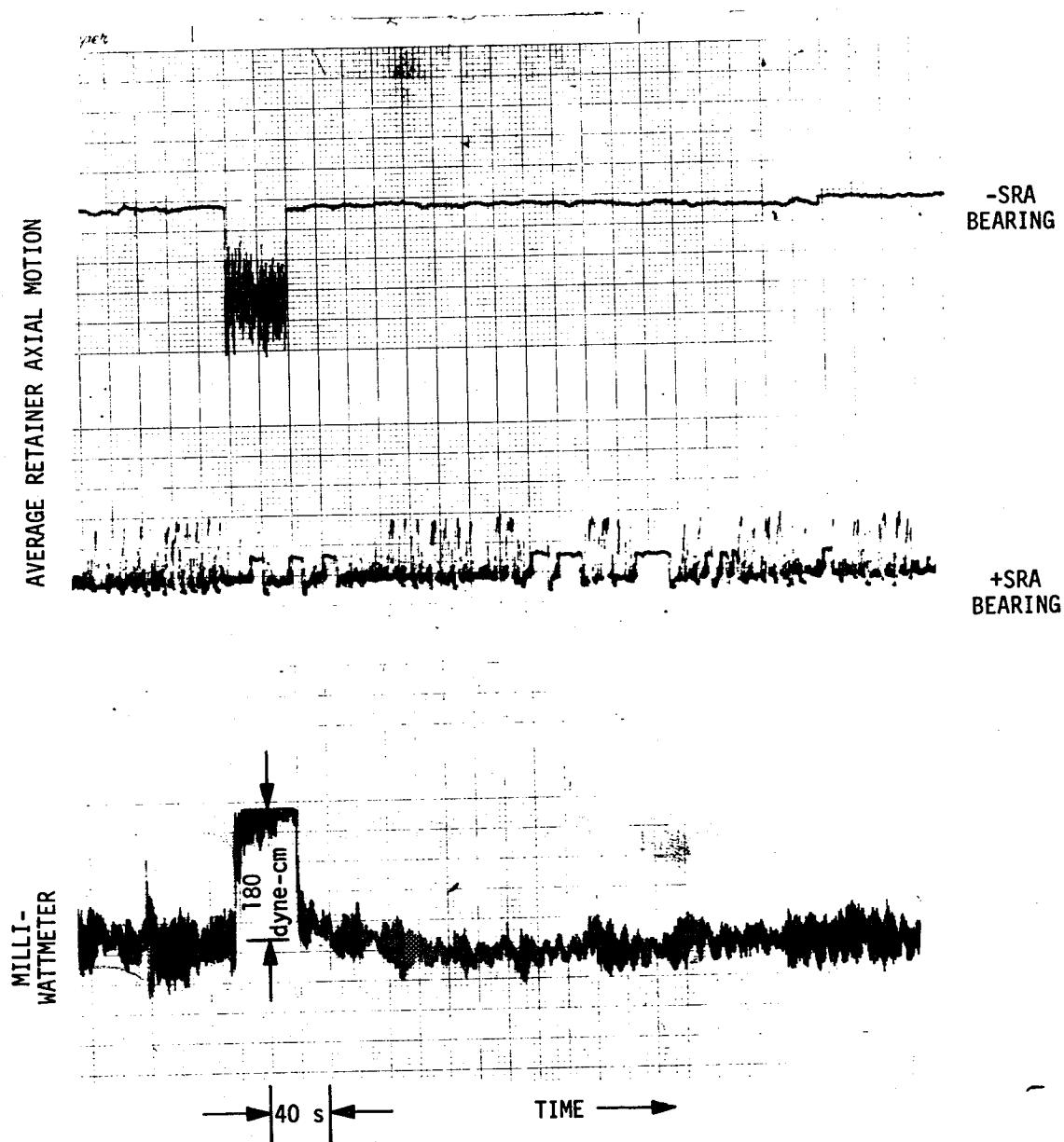
MILLI-
WATTMETER

180 dyne-cm

40 s

TIME ⟶

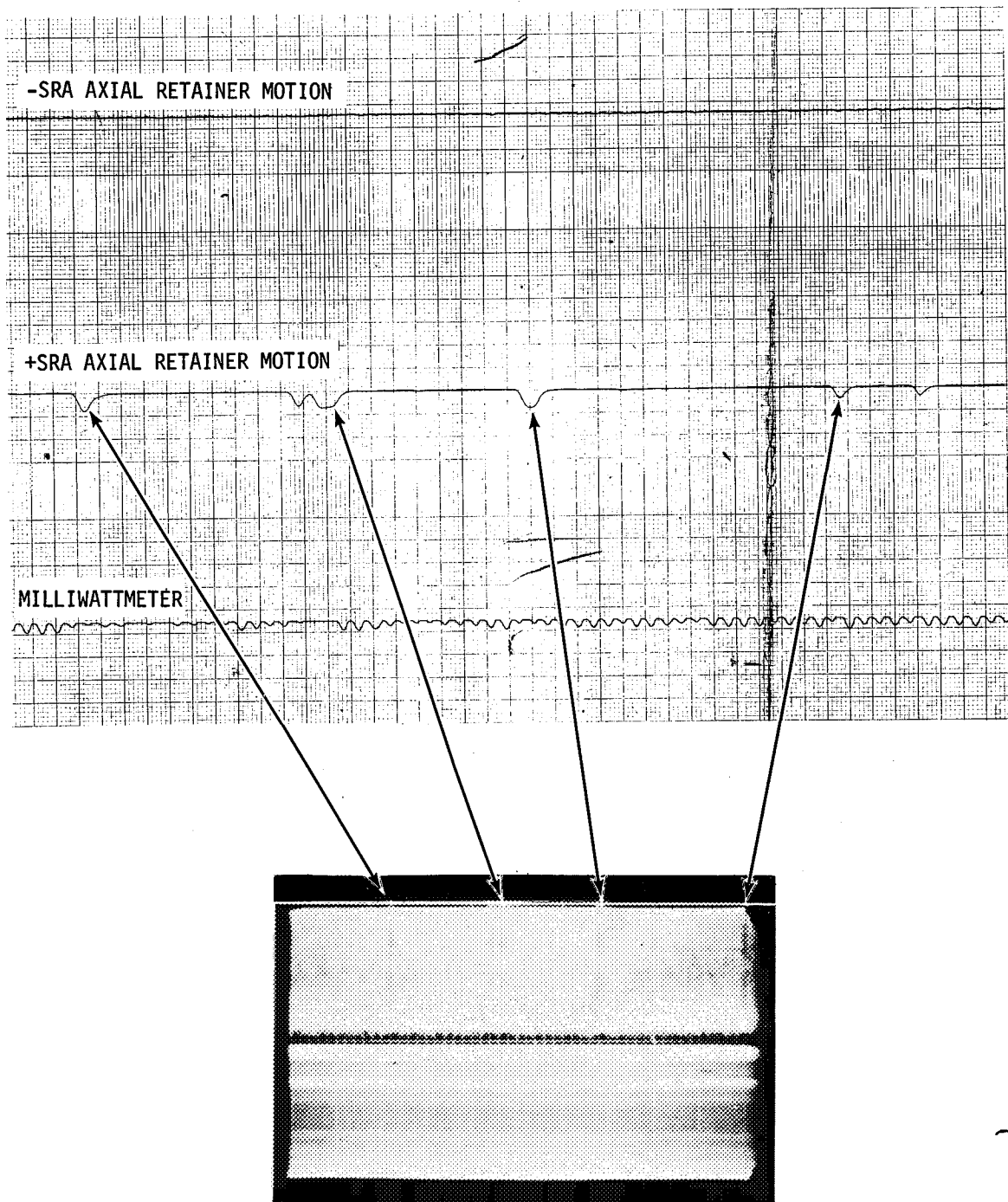Fig. 21.   Retainer-average-motion trace during bimode.

23

Fig. 22.   Retainer-average-motion trace compared with
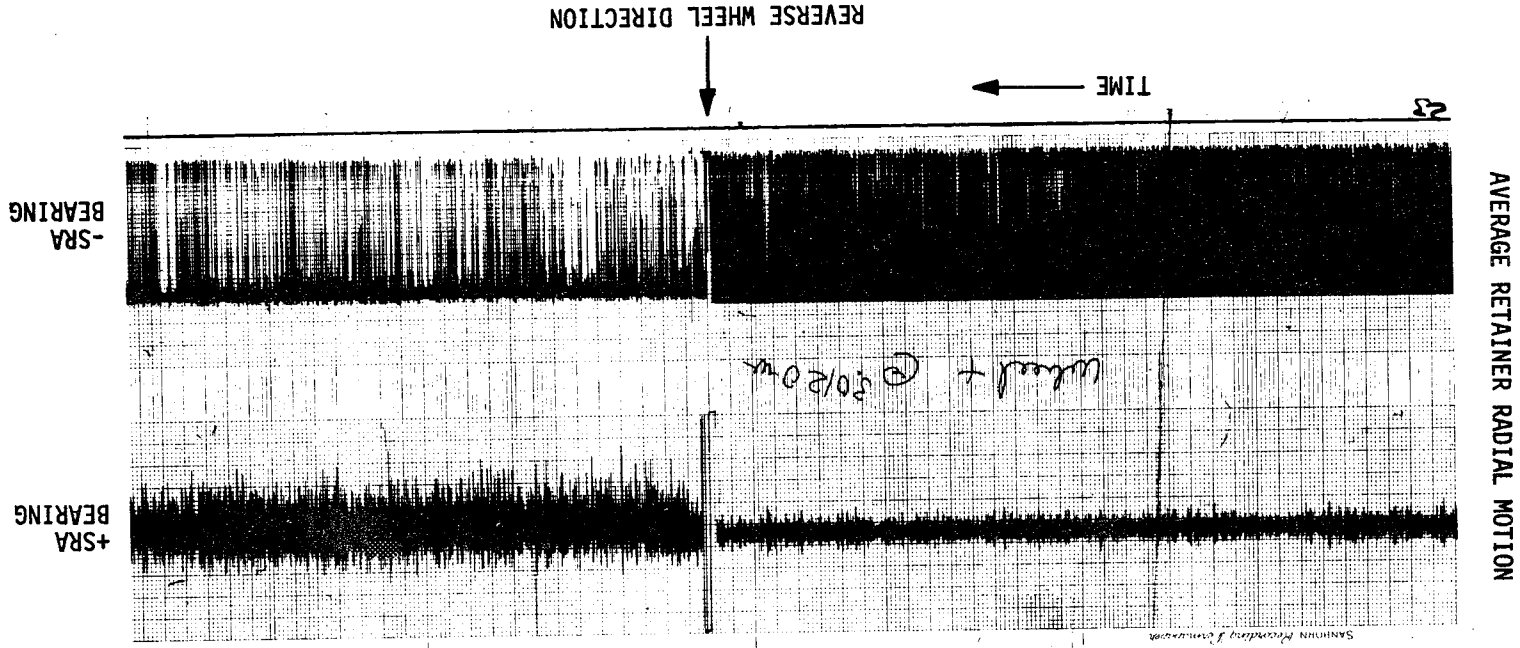actual motion and milliwattmeter trace.

Fig. 23. Retainer-average-motion trace for plus and minus rotation.

REVERSE WHEEL DIRECTION

TIME

AVERAGE RETAINER RADIAL MOTION

-SRA BEARING

+SRA BEARING

25

$$\omega_W = NW\dot{\beta} \qquad W = 1, 2, 3 \ldots \qquad (5)$$

where N is the number of balls in either bearing and W is an integer. Each of these signals is amplitude modulated at the corresponding multiple of the ball-group beat frequency

$$\dot{\xi}_W = NW\dot{\epsilon} \qquad (6)$$

showing that both bearings are involved in producing the signals.

The vectors representing these signals do not rotate about the spin axis, but are fixed with respect to the stationary races. Hence, the maximum observed amplitudes depend on how the races happen to be mounted with respect to each other, and how the shaft happens to be mounted in the test rig.

The lowest frequency output, W = 1, has been called "ball beat", apparently because of its amplitude modulation. A better name might be ball pass, since combinations like ball-beat beat period become ball-pass beat period, and because the effect is evidently the result of individual balls passing a disturbance in the stationary-race wear tracks.

4.2   Experimental Observations

The ball-pass forces are easily demonstrated by mounting a pair of bearings as in Fig. 24. The end view in Fig. 24 is meant to indicate that the ends of the shaft are restrained to move in the OXY plane; only force components in the YY direction are measured.
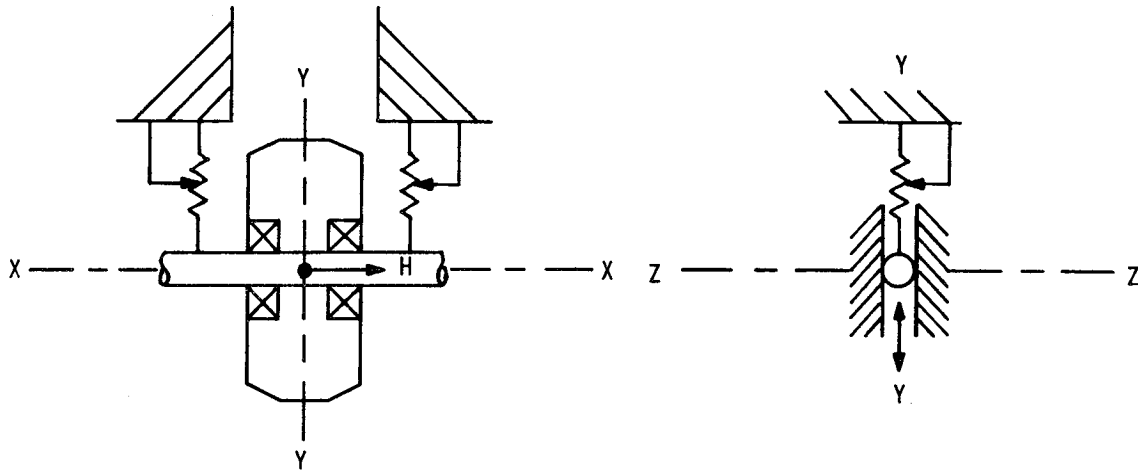

Fig. 24.   Ball-pass test fixture.

Using the apparatus of Fig. 24 and the same races for all tests, ball-pass signals were investigated for N = 3, 4, 6, 8, 9, and W = 1, 2, 3, 4 at a $\dot{\beta}$ of 143 Hz (chosen to avoid multiples of 60). ω_W values for these conditions are given in Table 1.

Table 1. ω_W for $\dot{\beta} = 143$ Hz.

ω_W / N	1	2	3	4
3	429	858	1287	1716
4	572	1144	1716	2288
6	858	1716	2574	3432
8	1144	2288	3432	4576
9	1287	2574	3861	5148

These numbers fall into the audio-frequency range. It was found that tones at these frequencies could invariably be heard amongst the general background noise coming from the assembly, and that beats in these tones could also be heard. In fact, these tones and beats were clearly identified with the "ringing" which accompanies small-ball-bearing operation -- often noted, never explained. When picked up with a microphone and examined, these tones and beats were indistinguishable (except for amplitude) from the shaft velocity outputs at the same frequencies. To demonstrate all these effects, the recording system of Fig. 25 was adopted. The two lowest frequency ball-pass signals were obtained using velocity pickoffs at the shaft ends, and the next two acoustically with a microphone. Counters, oscilloscopes, and a miniature computer were liberally used to keep track of the various frequencies. Figure 26 (Sheet 1) shows the first four ball-pass signals for a four-ball assembly as measured on this system. Sheet 2 of Fig. 26 shows the ω_3 audible signal compared with the ball-group unbalance signal (which is at $\dot{\beta}$) for a nine-ball assembly. In every case, Eq. (6) applies, although the highest audible (W = 4) in Fig. 26 (Sheet 1) is slightly muddled. Figure 27 plots the maximum amplitude (arbitrary units) for the ω_1 signal in a series of experiments with a nine-ball assembly versus the rotational position of the shaft (shaft angle) as mounted with respect to the measuring axis. The various runs were conducted with different amounts of inner-race misalignment, and demonstrate no dependence on this geometrical defect. However, the signals pass through two maxima in one relative rotation, demonstrating nonrotation in space.
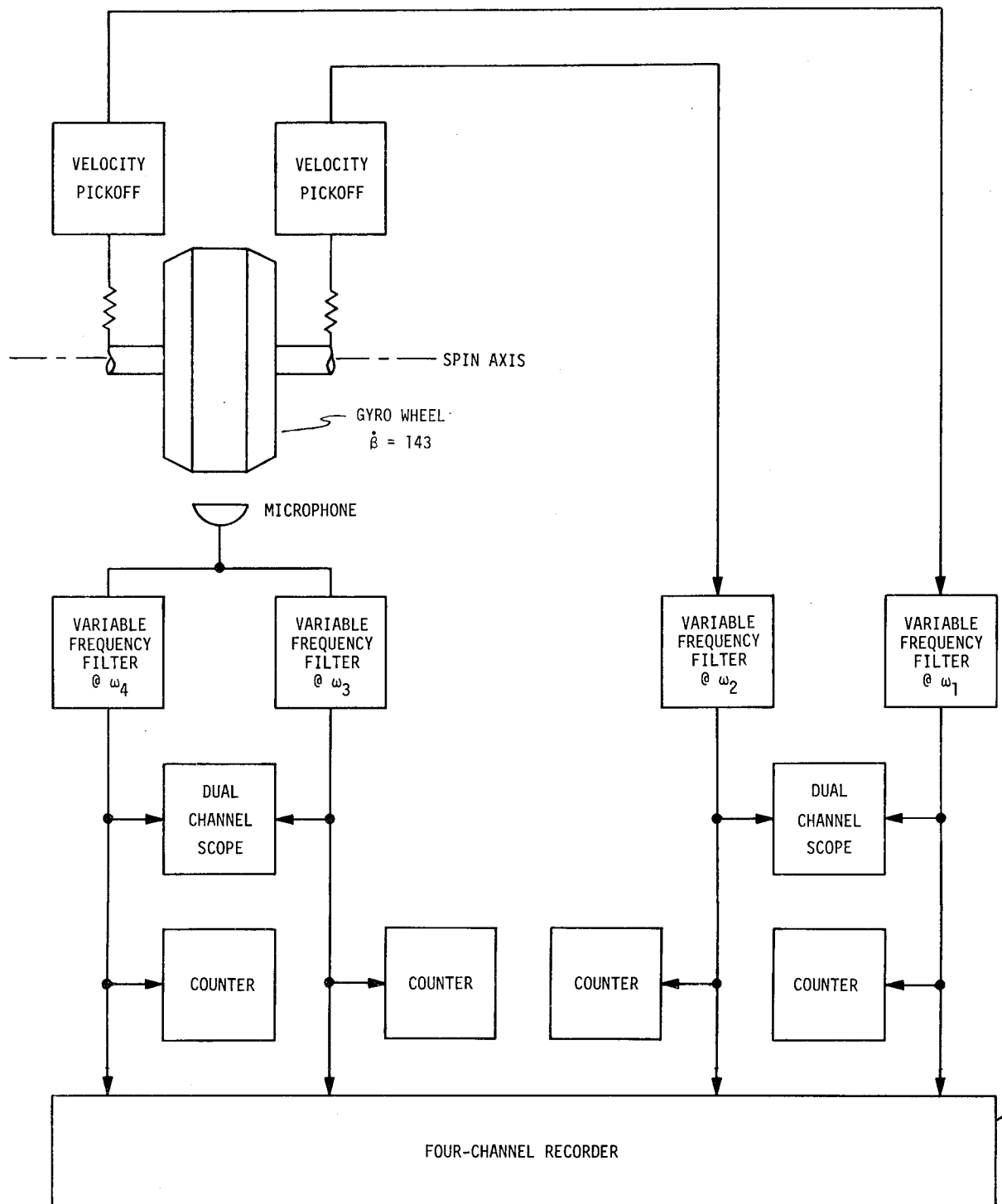
Fig. 25.   Ball-pass recording system.

4.3   Source of the Ball-Pass Signal

Both the frequencies and the nonrotation of the ball-pass signals suggest that they are caused by individual balls passing some sort of geometrical disturbance on the stationary race. The features ought to be small compared to the angular separation of the balls (40 degrees for N = 9), and repetitive to excite the higher ball-pass frequencies. They should also be capable of change with time since it was noticed that both the audible ringing and the various ball-pass amplitudes may change, especially after the introduction of new oil into the wear track. Figure 28 shows such a change in the amplitudes of the ω_3 and ω_4 signals from a nine-ball assembly as measured over 8 hours (temperature equilibrium for the apparatus is reached in 1/2 hour). All these considerations suggest that local variations in the wear track and starved EHD oil film should be investigated for their connection with ball-pass signals.

4.4   Dry Spots and Oil Retraction

One topographical feature of the wear track possessing these characteristics is the dry spot or oil-retraction phenomenon which has been observed in many bearings after running.[8]   Local areas have been noted where the residual surface oil does not wet the wear track. Figure 29 shows photographs of typical dry spots. They subtend arcs of 2 or 3 degrees, are repetitive, are longer in the roll direction than the Hertz width (1 degree in this bearing), are 50 to 100 microinches deep with respect to the residual oil, and have been observed to persist through several run-disassembly cycles.

A detailed hypothesis of how dry spots could cause the ball-pass signals will not be given here. However, a series of experiments which show a connection between the signals and the surface-energy state of the wear track will be discussed in order to make the concept plausible.

Figure 30 plots the ω_1, ω_2, ω_3, and ω_4 signal amplitudes (arbitrary units) versus shaft locating angle for a series of tests of a nine-ball assembly. Between the runs, the surface energy of the wear track was altered as per the following schedule.

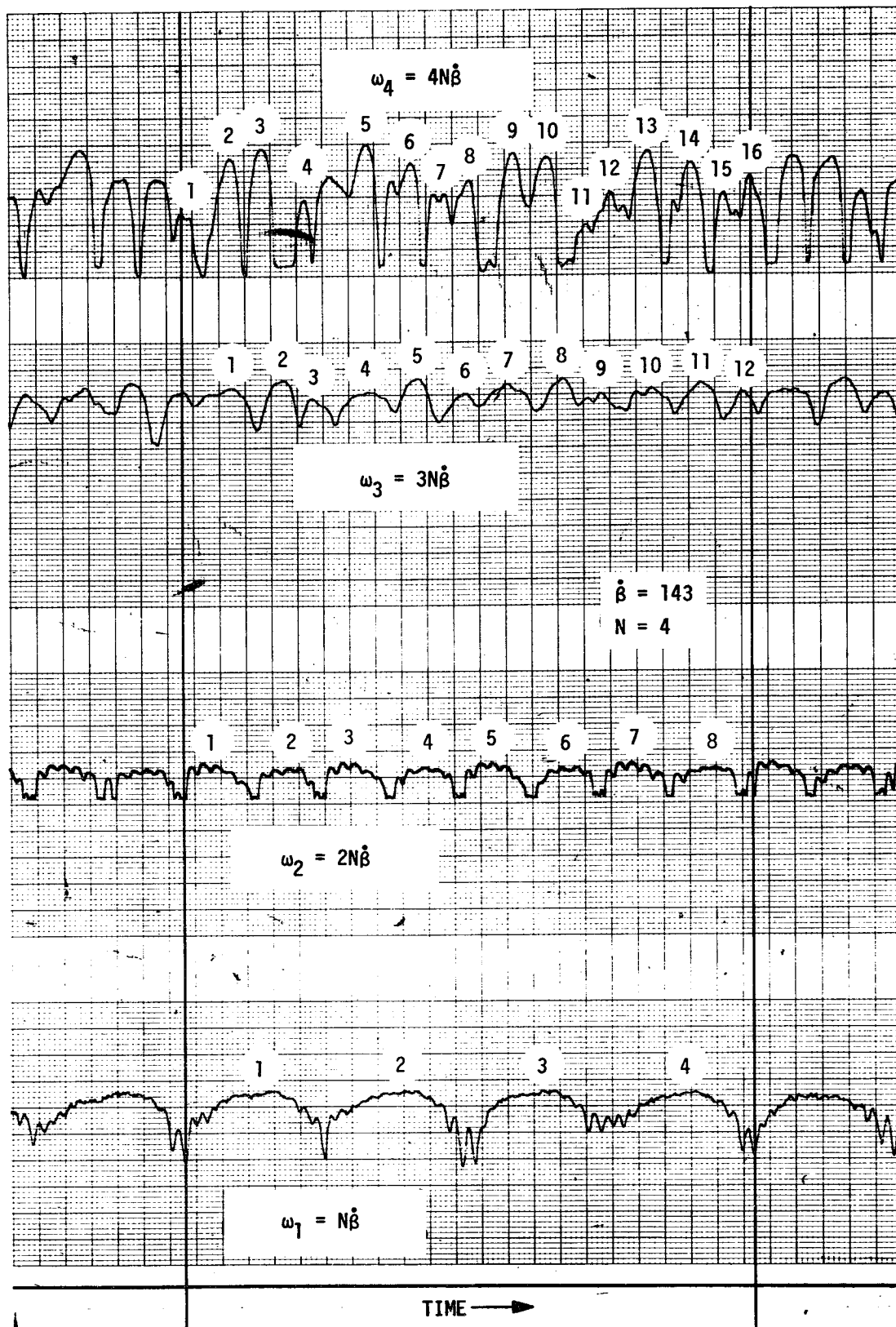|	
Run 1:	Typical wear track lubricated with 200 cp mineral oil.
Clean 1:	None.
Run 2:	Repeat of run 1 to check reproducibility.
Clean 2:	Solvent (Freon) removes bulk lubricant, does not remove any physically absorbed material from stainless steel.

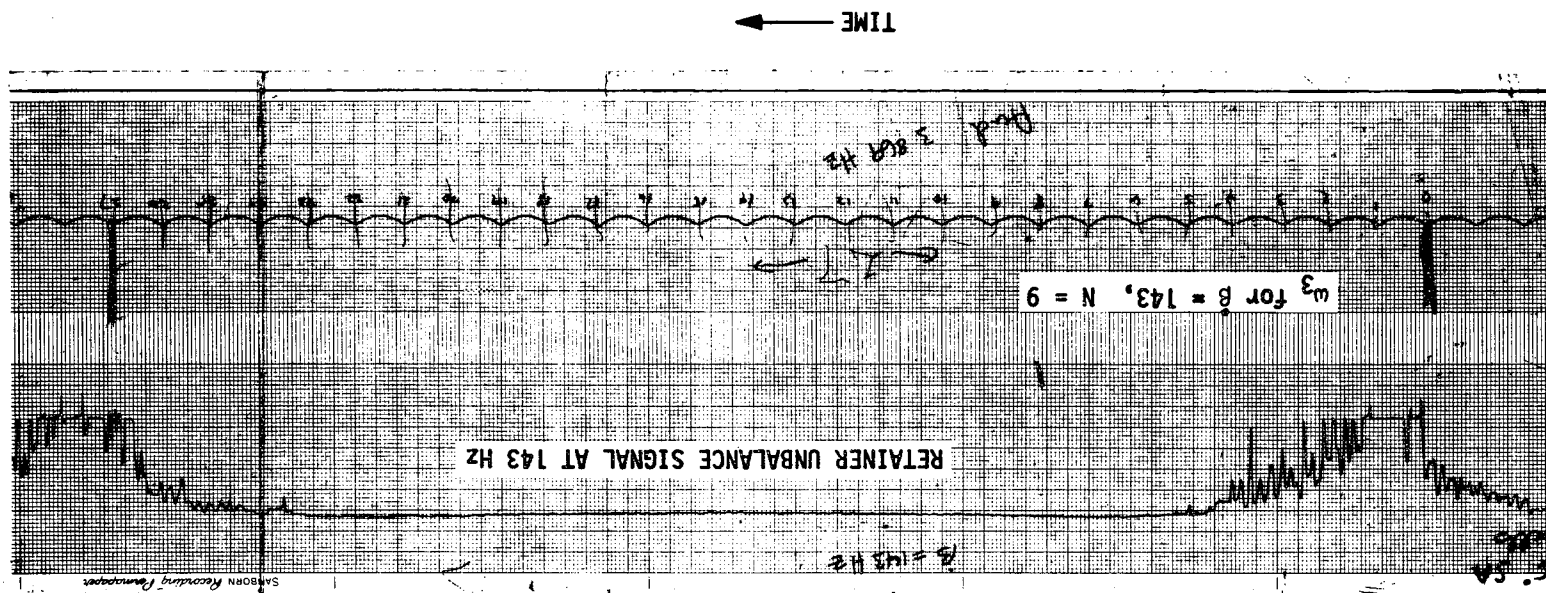Fig. 26.   Ball-pass signals (Sheet 1 of 2).
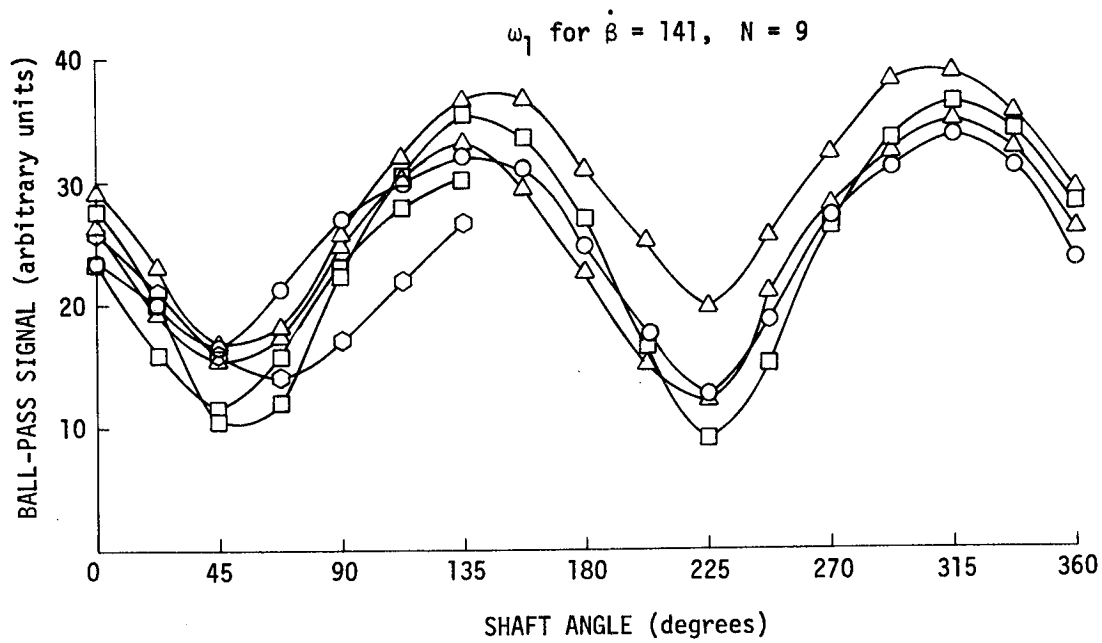
Fig. 26.   Ball-pass signals (Sheet 2 of 2)

TIME

ω_3 for β = 143, N = 9

RETAINER UNBALANCE SIGNAL AT 143 Hz

β = 143 Hz

31

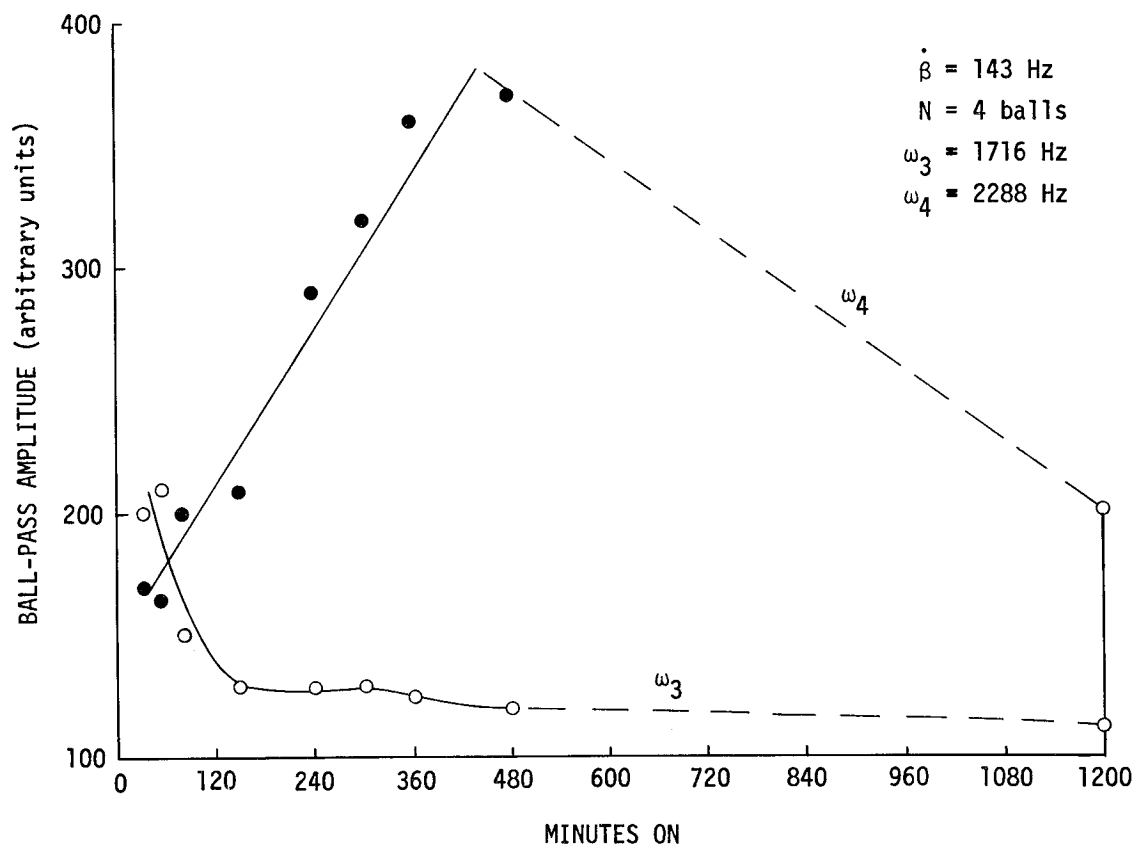Fig. 27.   Ball-pass amplitude versus shaft locating angle.

Fig. 28.   Ball-pass amplitude versus time.

Run 3:   Lubricated with solution of palmitic acid (a surfactant
             which will displace alkanes from stainless-steel
             surfaces, and which is also a good boundary lubricant
             in n-hexadecane.

Run 3A: Partial repeat of run 3.

Clean 3:   Solvent (Freon) removes bulk lubricant, does not
             remove any physically absorbed material.

Run 4:   Lubricated with 200-cp mineral oil.

Clean 4:   Solvent (Freon) removes bulk lubricant, acid (concen-
             trated sulfuric and chromic) removes any physically
             absorbed organic species.

Run 5:   Lubricated with 200-cp mineral oil.
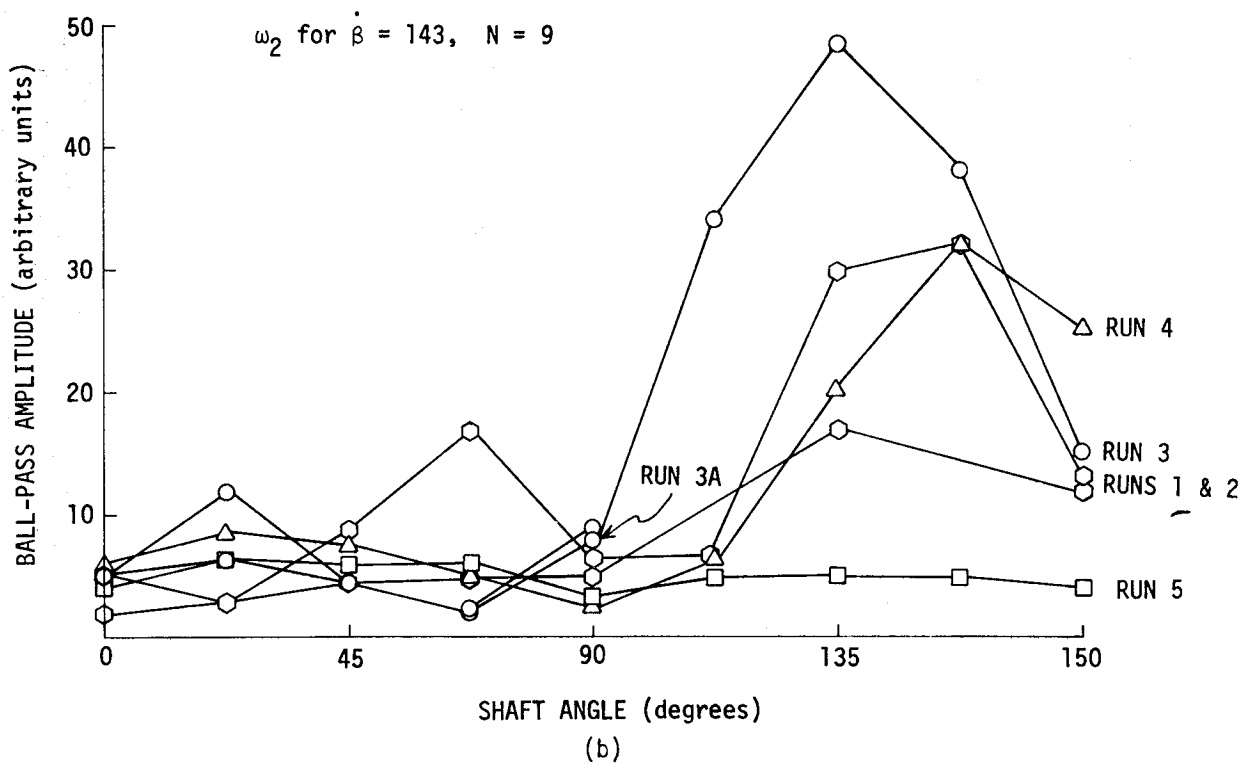

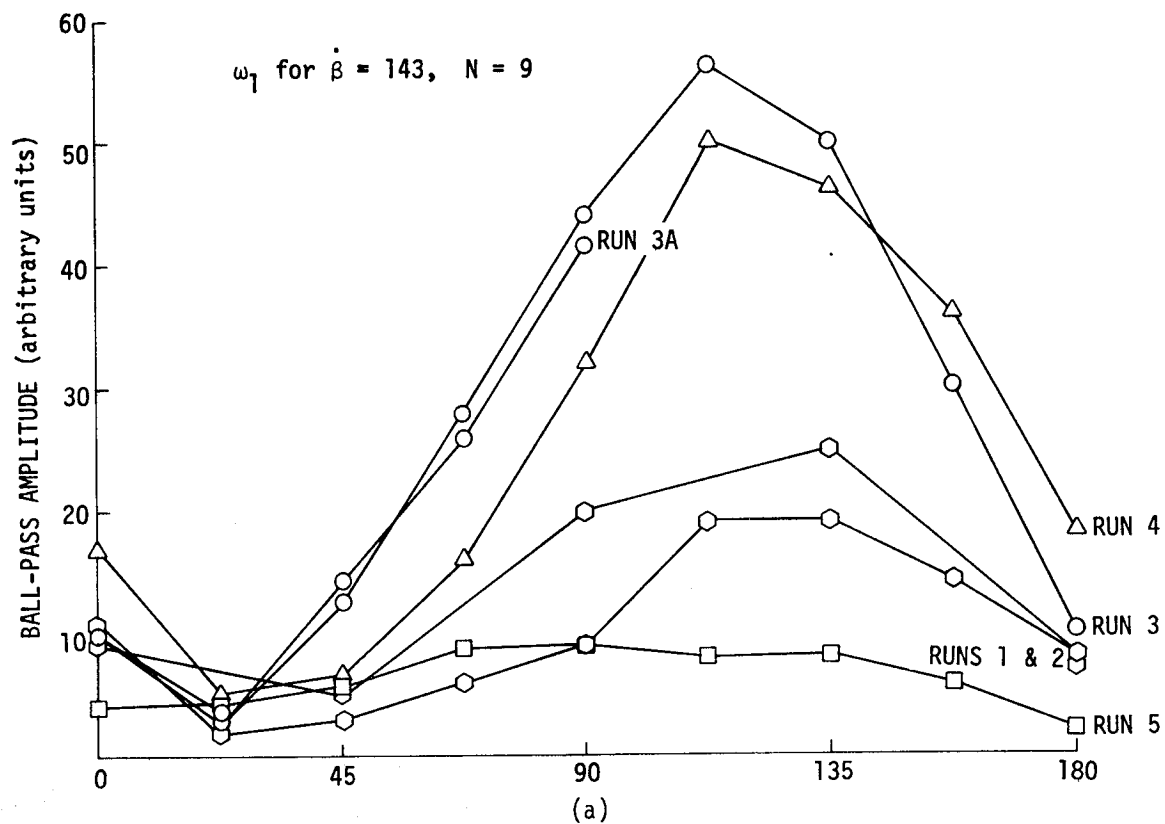Fig. 29.   Dry spots.

Fig. 30.   Ball-pass signals for various surface energies
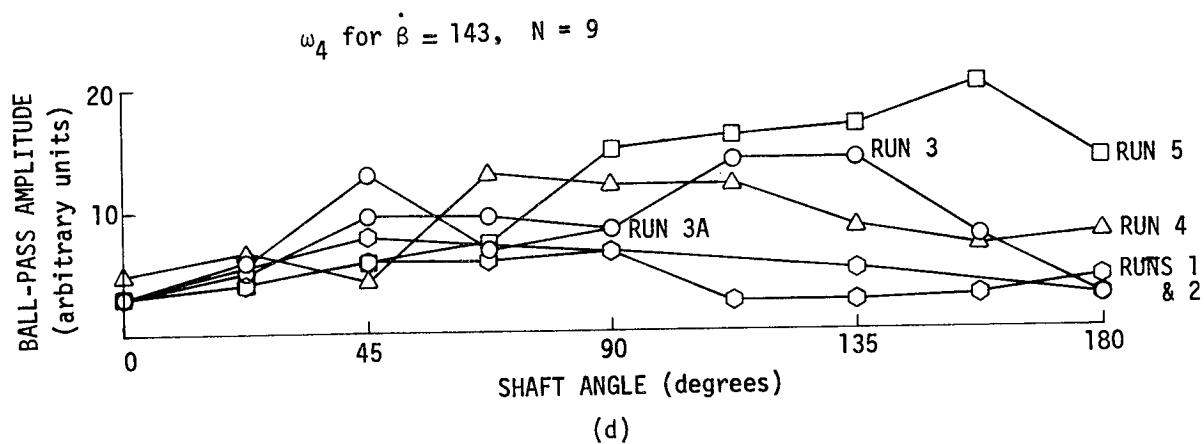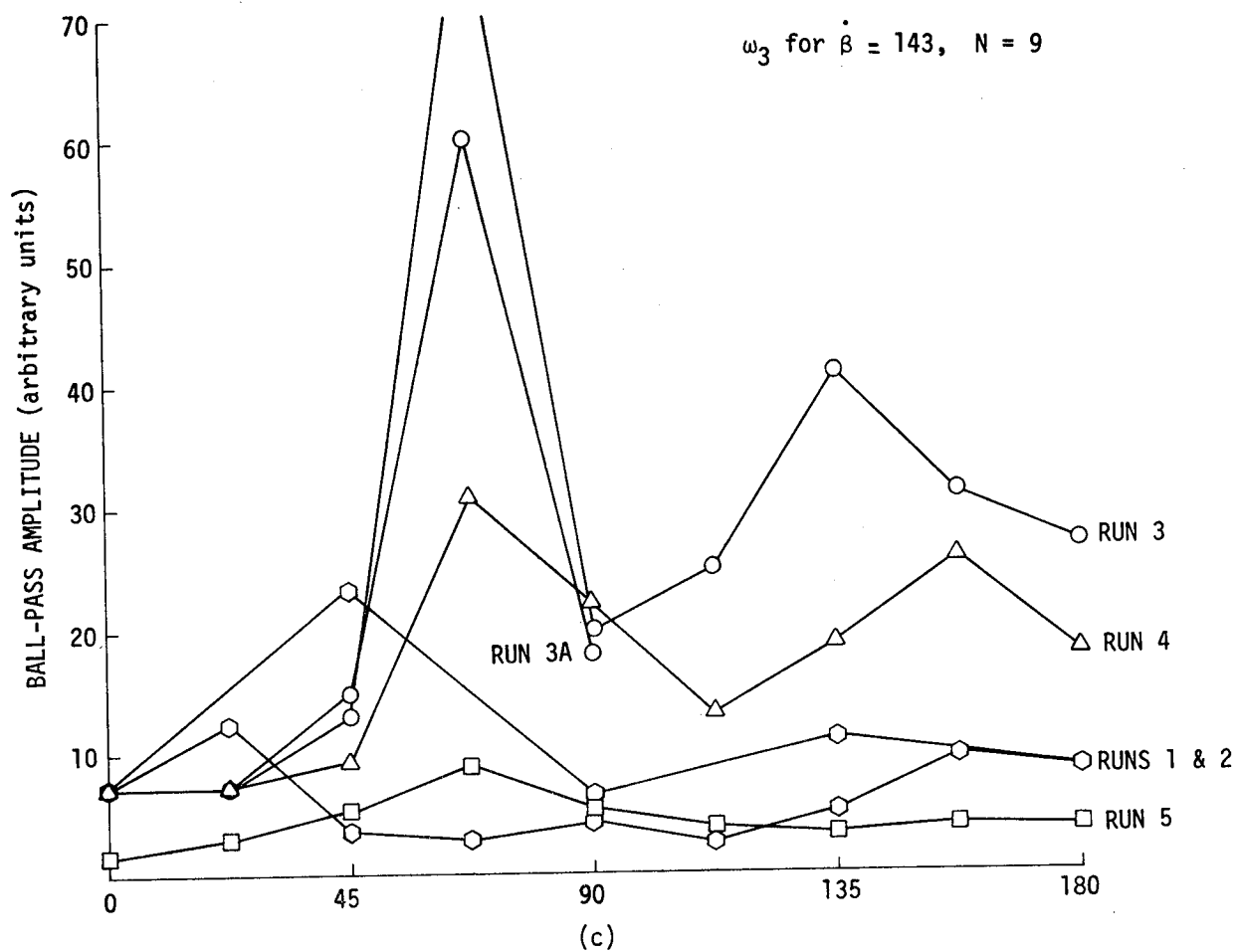   on the wear track (Sheet 1 of 2).

Fig. 30.   Ball-pass signals for various surface energies
on the wear track (Sheet 2 of 2).

Consider the ω_3 amplitudes in Fig. 30. They can be interpreted as showing that palmitic acid displaced the mineral oil from the wear track so as to form a series of dry spots in the 70-degree region of one race. These spots had the proper average size and spacing to excite the ω_3 frequency strongly. The spots remained through a solvent cleaning and relubrication with mineral oil. They were removed with the subsequent acid clean, leaving a relatively smooth wear track for ω_3 excitation.

Results for the other ball-pass frequencies can be similarly interpreted. Thus, it seems that something can be inferred about the local state of the wear track and EHD film merely by listening to the assembly.

LIST OF REFERENCES

1. Kingsbury, E. P., <u>Oil-Film-Parameter Investigation</u>, Charles Stark Draper Laboratory Report E-2650, April 1972.

2. Wedeven, L. D., D. Evans, and A. Cameron, "Optical Analysis of Ball Bearing Starvation", <u>Trans.</u>, ASME, JOLT 93F, No. 3, 1971.

3. Ray, R. E., and E. Zeigler, <u>Hydrodynamic Lubrication Improvement in Ball Bearings</u>, Report #PPD-72-E-10326, 1972, Northrop Corp., Norwood, Mass.

4. Wedeven, L. D., personal communication.

5. Kingsbury, E. P., "Ball Motion in Angular Contact Bearings", <u>Wear</u>, 11, p. 41, 1968.

6. Horsch, J. D., "Correlation of Gyro Spin-Axis Ball Bearing Performance with the Dynamic Lubricating Film", <u>ASLE Trans.</u>, 6, p. 112, 1963.

7. Kingsbury, E. P., "Experimental Observations on Instrument Ball Bearings", <u>Bearing Conference Proceedings</u>, Dartmouth College, Hanover, N.H., 1968.

8. <u>Final Report, Gyro Bearing Improvement Program</u>, Charles Stark Draper Laboratory Report R-674, 1970.

DISTRIBUTION LIST

Internal:

R. Booth

E. Carbrey

W. Denhard

A. Edwards   (5)

J. Feldman

A. Freeman

J. Gilmore

E.C. Hall

D. Hoag

L. Hughes

E. Kingsbury   (6)

R. Morey

P. Palmer

R. Price   (2)

R. Ragan

R. Schiesser

N. Sears

H. Singer

Apollo Library   (2)

DL Library   (10)

External: (19 + 1 R)

Malcolm E. Jones (EG-261)
NASA/JSC
Guidance & Control Division
2101 Webster Seabrook Road
Houston, Texas 77058

Apollo Document Group   (18 + 1 R)
NASA/JSC
Mail Station BM 86
Houston, Texas 77058